Ore Geology Reviews 56 (2014) 234–257

Contents lists available at ScienceDirect

Ore Geology Reviews

journal homepage: www.elsevier.com/locate/oregeorev

Geology, mineralogy, and geochemistry of the Vazante Northern Extension zinc silicate deposit, Minas Gerais, Brazil

Paul R. Slezak [a,*], Gema R. Olivo [a], Gustavo Diniz Oliveira [b], Marcel A. Dardenne [c,1]

[a] Department of Geological Sciences and Geological Engineering, Queen's University, Kingston, ON K7L 3N6, Canada
[b] Exploração Mineral, Votorantim Metais, Praça Ramos de Azevedo, 254, São Paulo, Brazil
[c] Instituto de Geociências, Universidade de Brasília, D.F., Brazil

ARTICLE INFO

Article history:
Received 7 March 2013
Received in revised form 28 May 2013
Accepted 26 June 2013
Available online 3 July 2013

Keywords:
Willemite hypogene ore
Non-sulfide zinc deposits
Neoproterozoic carbonate sequences
Vazante Group
Brasília Fold Belt
Lithogeochemistry
Base metal mineralization

ABSTRACT

The Vazante Northern Extension orebodies (850 kt at 16% Zn) are the continuation of the structurally controlled, hypogene, non-sulfide zinc orebodies of the Vazante deposit (18 Mt at 19% Zn), Minas Gerais, Brazil. The Vazante orebodies are hosted in the dolomitized carbonate rocks of the Serra do Poço Verde Formation that were deposited in an intertidal to supratidal environment. The Serra do Poço Verde Formation is part of the Neoproterozoic Vazante Group, which is located in the Brasília Fold Belt along the western margin of the São Francisco Craton. The Northern Extension orebodies occur within major tectonic-hydrothermal breccias controlled by a NE-trending fault zone. The faults and the breccias are interpreted to be formed during the so-called D_2 deformation event, which is related to the Late Proterozoic Brasiliano Orogeny. The faults were reactivated during their evolution and are cut by later transcurrent faulting.

Four types of tectonic-hydrothermal breccia occur in the North Extension zone. Type 1 breccia is distal from the willemite ore and is comprised of weakly brecciated dolostone with Fe-carbonate alteration, whereas type 2 breccia exhibits strong Fe-bearing carbonate alteration (dolomite with 1.5 to 3.3 wt.% FeO and 0.3 to 1.25 wt.% ZnO) of the clasts, Fe-carbonate veinlets, a more intense brecciation of the clasts, and has overprinted the type 1 breccia. Type 3 breccia is composed mainly of hematite that replaced previously altered dolomite clasts and filled the breccia matrix. Type 4 breccia, which is typically proximal to type 3 breccia, is the willemite ore breccia which contains three generations of hypogene willemite as well as hematite, franklinite and minor amounts of quartz and ferroan (~1.99 wt.% FeO) and zincian (~2.65 wt.% ZnO) dolomite. Type 4 breccia commonly occurs in lenses surrounded by the type 3 hematite breccia, and willemite partially replaces hematite and altered carbonate clasts and fills breccia matrix and veinlets. In the southern part of the deposit, late sulfide-rich veinlets with galena, sphalerite, native silver, covellite, and stromeyerite cut the hypogene zinc silicate mineralization.

Lithogeochemical analysis and mass-balance of the hydrothermal breccia were used to evaluate metals added during the hydrothermal period. The data show that the ore-related elements have been added to the system since the formation of the earliest breccia (Type 1 breccia). However, the type 3 breccia contains the highest average concentrations for As, Ba, Be, Bi, Fe, Ge, In, Mo, Ni, Sb, U, V, and W. Type 4 breccia is also enriched in the same elements and contains the highest average concentrations of Ag, Cu, Hg, Pb, S, Se, SiO_2, and Zn. The evidence that the ore-related elements were added to the system during the formation of types 1 and 2 breccias, suggests that the metalliferous fluids were interacting with the host rocks, but were not able to effectively precipitate the ore-related elements. Important changes in the hydrothermal system would have increased its fugacity and pH allowing for formation, respectively, of type 3 hematite-rich breccia and type 4 willemite ore breccia, which are enriched in the other ore-related elements (e.g. As, Ba, Be, Bi, Cu, Fe, Ge, Hg, In, Mo, Ni, Pb, Sb, U, V, and W). These observations are consistent with a formation model proposed for the Vazante orebodies involving early interaction of metalliferous brines with the host rocks, followed by mixing of the metalliferous fluids with more oxidizing fluids, most likely meteoric water, leading to the precipitation of abundant hematite and willemite. Late, more reduced fluids formed the Pb, Cu and Ag-rich sulfide veinlets that cut the willemite mineralization.

1. Introduction

Since the early 20th century, zinc has been mainly produced from sulfide ores of sedimentary-exhalative (SEDEX), Mississippi Valley-type (MVT), Broken Hill-type (BHT), and volcanogenic massive sulfide (VMS) deposits due to the development of sulfide flotation

* Corresponding author. Tel.: +1 2503000421.
E-mail address: paul.r.slezak@gmail.com (P.R. Slezak).
[1] Deceased October 3, 2011.

0169-1368/$ – see front matter © 2013 Elsevier B.V. All rights reserved.
http://dx.doi.org/10.1016/j.oregeorev.2013.06.014

Table 1
Summary of the characteristics of major hypogene zinc silicate deposits in the world.

Deposits/ occurrences	Location	Size (Mt)	Grade (% Zn)	Host rocks	Host rock Age	Related structures	Ore minerals	Alteration	T_H (°C)	Salinity (eq. wt.%NaCl)	Associated elements
Beltana[a]	Australia	0.86	37.9	Limestone, dolostone	Cambrian	Beltana Fault, district scale folds, breccia, karst	Willemite, coronadite, hedyphane, mimetite, smithsonite	Ferroan dolomite, hematite, quartz	50–170	4–14	As, Be, Cd, Cu, Fe, Ge, Mn, Pb, Sb, V
Star Zinc[b]	Zambia	0.073[c] 0.118[d]	16.5[c] 21.58[d]	Dolostone	Neoproterozoic	Mwambeshi Shear zone, district scale fractures, karst	Sphalerite, willemite, galena, smithsonite, cerussite	Quartz, hematite,	160–240	8–16	Ag, Ba, Cd, Pb, Sb
Kabwe[e]	Zambia	12.3[f]	25.2[f]	Dolostone	Neoproterozoic	Mine Club Fault, district scale folds	Sphalerite, galena, willemite, smithsonite, cerussite	Quartz, dolomite, hematite, goethite, pyrite	257–385 75–200	15–31.6 11.5	Ag, Cd, Cu, Ga, Ge, In, Pb, V
Berg Aukas[g]	Namibia	3.4[f]	15[f]	Dolostone	Neoproterozoic	Berk Aukas syncline, district scale faults and folds	Willemite, sphalerite, descloizite, mottramite	Dolomite, calcite	97–205[h]	23[h]	Ag, Cd, Ga, Ge, Pb, V[h,g]
Abenab West[g]	Namibia	0.1[f]	25[f]	Dolostone	Neoproterozoic	Pipe-like kharst structures	Willemite, descloizite	Dolomite, calcite	n/a		n/a
Vazante Mine	Brazil	18[i]	19[i]	Dolostone	Neoproterozoic	Vazante Shear Zone, district scale folds, breccia[j]	Willemite, sphalerite, franklinite[k,i,j]	Quartz, ferroan and zincian dolomite, hematite[i]	65–180[k] 201–232[l]	3–15[k] 15–23[l]	Ag, As, Cd, Co, Cu, Ge, Fe, Ni, Pb, S, Sb, U, V[e]
Northern Extension[m]	Brazil	0.85	16	Dolostone	Neoproterozoic	Vazante Shear Zone, district scale folds, breccia	Willemite, franklinite	Quartz, ferroan and zincian dolomite, hematite[a]	n/a	n/a	Ag, As, Be, Bi, Cd, Cu, Fe, Hg, In, Mo, Pb, Sb, Se, V

[a] Groves et al. (2003).
[b] Boni et al. (2011).
[c] Eastern ore body.
[d] Western Ore body.
[e] Kamona and Friedrich (2007).
[f] Hitzman et al. (2003).
[g] Scheider et al. (2008).
[h] Pirajno and Joubert (1993).
[i] Monteiro et al. (1999).
[j] Monteiro et al. (2007).
[k] Dardenne and Freitas-Silva (1999).
[l] Monteiro (2002).
[m] Slezak (2012).

and smelting techniques (Boni and Large, 2003). However, the potential for producing zinc from high-grade non-sulfide deposits at lower costs using hydrometallurgical techniques has renewed the interest in non-sulfide zinc deposits around the world. These non-sulfide zinc deposits occur in two major subtypes: supergene and hypogene deposits (Hitzman et al., 2003).

Supergene zinc deposits can be further divided into three categories: direct replacement, wall-rock replacement, and residual karst-fill. These deposits are thought to have been created by the oxidation of MVT deposits. Direct replacement deposits form when zinc sulfide minerals, such as sphalerite, are oxidized and replaced by smithsonite and hemimorphite. Other secondary lead, copper, and iron oxides may also occur associated with zinc minerals. Wall-rock replacement deposits form near the original sulfide body as a result of groundwater leaching zinc from the sulfide body and precipitating it into the surrounding carbonate host rocks. Residual karst-fill deposits are the result of zinc minerals accumulating in karst depressions and caves that were formed due to a weathering environment (Hitzman et al., 2003).

Hypogene non-sulfide zinc deposits, herein referred to as hypogene zinc silicate deposits, are precipitates of hydrothermal fluids that can be either structurally-controlled or stratiform (e.g. Franklin, NJ). The world's most preeminent examples of structurally controlled deposits are the Beltana–Aroona Belt of South Australia, the Otavi Mountainland deposits of Namibia, the Zambezi Metamorphic Belt, and the Vazante and Vazante-Northern Extension deposits in Minas Gerais, Brazil, which are hosted within brecciated carbonate rocks and where zinc occurs mainly as willemite (Table 1).

Hypogene zinc silicate deposits occur in Neoproterozoic to Cambrian age passive-margin sedimentary basins usually associated with low grade metamorphism. These deposits are hosted in carbonate rocks associated with major structures, such as district scale faults and folds (e.g. Beltana, Vazante, and Kabwe districts). Brecciation is commonly associated with mineralization such as the case with the Vazante trend mineralization. The breccias at Beltana and Star Zinc are associated with karst (Boni et al., 2011; Groves et al., 2003); whereas the breccias at Vazante, Kabwe, and Abanab West are a result of tectonism and hydrothermal fluid flow (Dardenne, 2000; Kamona and Friedrich, 2007; Scheider et al., 2008; Slezak, 2012).

All of the deposits are dominated by mineralogical associations containing the zinc silicate, willemite, as well as zinc oxides, such as zincite, franklinite, and varying amounts of sphalerite. Ferroan dolomite, hematite, and quartz are all common alteration minerals found in these types of deposits. Additionally, all of the deposits show a range of fluid inclusion homogenization temperatures (T_H) of 50–385 °C with salinities ranging from 3 to 31.6 eq. wt.% NaCl (Table 1).

The Vazante orebodies are among the world's largest hypogene zinc silicate deposits with estimated reserves of 18 Mt at 19% Zn additional reserves of 850 kt of ore at 16% Zn in the Northern Extension deposits (Votorantim, pers. commun., 2011). The Vazante and Northern Extension deposits are located in the southern region of the Brasília Fold Belt near the town of Vazante, Minas Gerais. They are hosted by the Neoproterozoic Vazante Group, which also comprises the sulfide zinc-lead deposits in the northern region, near to the town of Paracatú (e.g., Morro Agudo mine: Misi et al., 2005; Monteiro et al., 2007). The zinc silicate orebodies were locally mined in the 1950s for the secondary "calamine" (hemimorphite and smithsonite) zinc ore. Artisanal mining was followed by open pit mining in beginning in 1969 and by underground mining beginning in 1983, focusing mainly on the hypogene ore (Monteiro et al., 1999).

The underground and pit exposures and extensive drilling provide ideal conditions to conduct a detailed investigation of the mineralized zones and host rocks. Previous studies include Rigobello et al. (1988) and Dardenne (2000), which first described the stratigraphy and host rocks as well as the regional tectonic and local structural setting of the Vazante mine. Monteiro et al. (1999, 2006, 2007) studied the mineralization, alteration, fluids, and stable isotopes of the Vazante mineralization and suggested that it formed by the mixing of an oxidizing, hot, sulfur-deficient metalliferous fluid with cool, meteoric water. Dardenne and Freitas-Silva (1999) investigated the fluids associated with the main Vazante mineralization and concluded that the fluids had salinities of 3–15 eq. wt.% NaCl and homogenization temperatures ranging from 65 to 180 °C. Lead isotope investigations by Dardenne and Freitas-Silva (1999), Misi et al. (2005), and Cunha et al. (2007) suggested galena ranges in age from 1.8 to 0.65 Ga. The 1.8 Ga dates are interpreted to be from radiogenic galenas derived from the São Francisco Craton and the Goiás Massif (Misi et al., 2005). The younger, 0.65 Ga, galenas are thought to have resulted from sulfide remobilization (Dardenne and Freitas-Silva, 1999).

However, major questions remain concerning the evolution of the Vazante system and the relevance of the various hydrothermal and deformational events involved in the formation of the silicate ore at these structurally controlled, carbonate hosted depositional sites. Why are these zinc silicate deposits confined to the southern part of the Vazante Group whereas lead–zinc sulfide deposits are common in the northern part? What are the factors controlling silicate zinc deposition at these sites?

This study focuses on understanding the major structural controls and the evolution of the hydrothermal alteration of the Northern Extension orebodies of the Vazante deposit, based on detailed mapping, petrography, mineralogy and lithogeochemistry. It aims to further our knowledge of the critical factors that allowed for the formation of the silicate zinc ore in these specific sites, and integrate these findings with data on similar deposits worldwide, in order to improve the exploration strategies for this type of deposit.

2. Regional geology

The Vazante and Northern Extension deposits are located in the Brasília Fold Belt along the western margin of the São Francisco Craton. This fold belt is roughly 1000 km long and is one of three fold belts in the Tocantins Province (Fig. 1A), which also includes: the Araguaia Belt on the eastern margin of the Amazonia Craton, the Paraguay Belt on the southeastern margin of the Amazonia Craton (Almeida et al., 1981; Pimentel et al., 2001; Rodrigues et al., 2010; Valeriano et al., 2008).

The Brasília Fold Belt was created through a series of tectonic events starting with continental rifting of the São Francisco Craton c.a. 1700 Ma and ending with the Brasiliano Orogeny (Martins-Neto, 2009; Misi et al., 2005). The continental rift system evolved into a passive margin setting along the western edge of the São Francisco Craton, allowing for the deposition of intracratonic siliciclastic sediments and platform carbonates represented primarily by the Canastra-Paranoá-Vazante Groups at around 1200–900 Ma (Martins-Neto, 2009; Valeriano et al., 2008). The Vazante Group is the host of the Vazante and Northern Extension zinc silicate deposits.

Subduction of oceanic crust from the Brazilide Ocean beneath the São Francisco Craton began around 900 Ma, causing magmatism that would lead to the formation of the Goiás magmatic arc (Dardenne, 2000; Martins-Neto, 2009; Valeriano et al., 2008). Continuing subduction leads to the convergence of the Goiás magmatic arc and the São Francisco Craton around 850–750 Ma, which was the start of the Brasiliano orogeny. During this collision, the passive margin sediments were thrust as thin-skinned nappes onto the São Francisco Craton (Dardenne, 2000; Martins-Neto, 2009; Valeriano et al., 2008), and reached a metamorphic peak around 650 Ma (Martins-Neto, 2009). Dardenne (2000) also notes geochemical and isotopic evidence of a late Brasiliano collisional event c.a. 630–610 Ma, interpreting it as the last stage of convergence of the Goiás magmatic arc with the São Francisco Craton.

The southern region of the Brasília Fold Belt is comprised of the Ibiá, Canastra, Vazante, and Bambuí Groups (Table 2). The Ibiá, Canastra,

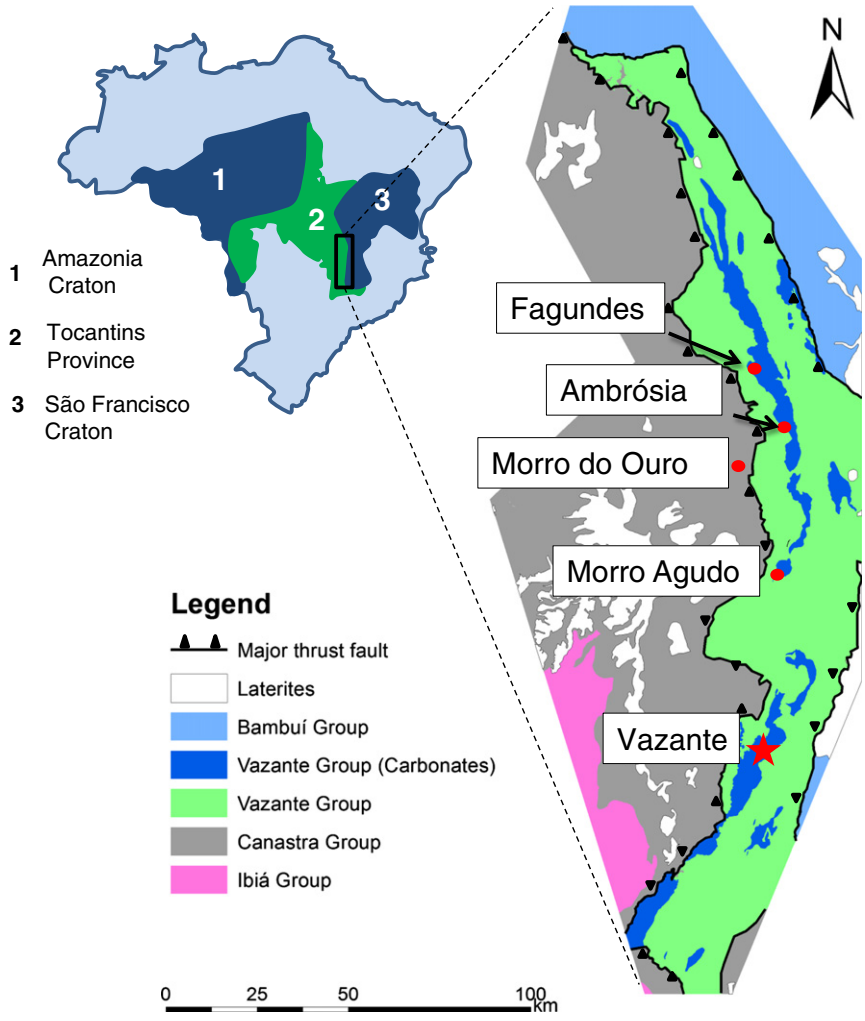

Fig. 1. A) Map of Brazil showing the location of the Tocantins Province. B) Map of the southeastern part of the Brasília Fold Belt within the eastern margin of the Tocantins Province, highlighting the major units and mineral deposits in the region.
Modified from Monteiro et al. (2006), (2007), and Votorantim Metals (pers. commun., 2011).

Vazante Groups form a complex system of nappes that are thrust onto the Bambuí Group sediments to the east (Dardenne, 2000). The Canastra, Vazante, and Bambuí Groups are the most prominent sedimentary units in the Vazante (southern) region (Fig. 1B). The Canastra Group hosts the world-class Morro do Ouro gold deposit. The Vazante Group (Fig. 2) hosts the Morro Agudo MVT/Irish-type Pb–Zn deposit, and the Ambrósia and Fagundes Pb–Zn sulfide occurrences in the northern Paracatú region (Hitzman et al., 1995, 2003; Misi et al., 2005; Monteiro et al., 2007). It also hosts various phosphate deposits in both northern and southern regions.

3. The Vazante Deposit: Geology and mineralization

The zinc silicate mineralization of the Vazante deposit is hosted in a tectonic-hydrothermal breccia zone found near the contact between the Lower Pamplona and Upper Morro do Pinheiro Members of the Serra do Poço Verde Formation of the Vazante Group (Monteiro et al., 1999, 2006, 2007; Rigobello et al., 1988). Metamorphosed dikes are tectonically imbricated with the carbonates and hydrothermal breccias in the main orebody. Mineralization within the breccia occurs along a fault that strikes N50E and dips 60–70° NW (Dardenne, 2000; Dardenne and Freitas-Silva, 1999; Monteiro et al., 1999, 2006, 2007). The fault is interpreted as an early syn-sedimentary growth fault that underwent multiple reactivations during the Brasiliano Orogeny, including reverse faulting during compression that later evolved into a normal, sinistral fault at the end of the orogenic event (Dardenne, 2000; Monteiro et al., 1999; Pinho, 1990). The fault zone in the Vazante deposit displays features typical of both brittle and ductile deformation, represented by brecciation and a weak schistosité-cisaillement (S-C) fabric, respectively (Monteiro et al., 1999). The Vazante ore body is nearly 5 km long and variably tens of meters thick, extending over 400 m below the surface.

The hydrothermal alteration within the Vazante district is largely controlled by the structures related to brecciation. Siderite, ankerite, quartz and hematite are common alteration minerals found in veins and filling spaces between breccia clasts. Rare gahnite also occurs in some veinlets proximal to the ore (Monteiro et al., 1999). Alteration in the surrounding host rocks of the breccia includes a color change from gray to pink dolostones caused by hematite alteration and silicification of dolostone (Dardenne, 2000; Monteiro et al., 1999, 2006, 2007).

Willemite (Zn_2SiO_4) is the main zinc ore in the Vazante deposit. It occurs in pods, veinlets, and meter-wide veins within the tectonic-hydrothermal breccia and is controlled by antithetic faults in the deposit (Dardenne, 2000; Hitzman et al., 2003; Monteiro et al., 1999, 2006, 2007). According to Monteiro et al. (1999), small sulfide bodies

Table 2
Stratigraphic and age summary of the Ibiá, Canastra, Vazante, and Bambuí Groups. *Conophyton* ages are constrained to when this variety of stromatolites appears in the fossil record. The K–Ar dates are interpreted as metamorphic ages related to the Brasiliano Orogeny. Sm–Nd and U–Pb dates are interpreted to be from their sources rocks. The Re–Os dates are interpreted to be the maximum ages of deposition.

Sedimentary groups	Formations	Description	Geochronological Data (Ma)
Bambuí[a]	Três Marias	Arkoses and siltstones	650–600 (K/Ar and Rb/Sr)[b]
	Serra da Saudade	Sandy pelites	900–610 (U–Pb)[c]
	Lagoa do Jacaré	Dark gray platform limestones	
	Serra da Santa Helena	Carbonaceous pelites	
	Sete Lagoas	Pelitic carbonates grading into dolomites	
	Jequitaí Formation	Diamictite beds containing limestone clasts	
Vazante[a]	See Fig. 2	Platform carbonates and phyllites	1350–950 (*Conophyton* stromatlites)[d]
			2200–1800 (Sm–Nd)[c]
			1350–630 (U–Pb)[b]
			1100–993 (Re–Os)[e]
Canastra[f,a,g]	Chapada dos Pilões	Intercalated phyllites and quartzites	1000 (Sm–Nd)[c]
	Paracatú	Gray carbonaceous phyllite with quartzite lenses	
	Serra do Landim	Pale green to gray-green calc-phyllite to calc-schis[d]	
Ibiá [h,a]	Rio Verde	Calciferous phyllites with some intercalations of	1100–800 (U–Pb & Sm–Nd)[i]
	Cubatão	quartzite	
		Diamictites	

[a] Dardenne (2000).
[b] Rodrigues et al. (2010).
[c] Thomaz Filho et al. (1998).
[d] Cloud and Dardenne (1973).
[e] Azmy et al. (2008).
[f] Almeida (1969).
[g] Freitas-Silva and Dardenne (1994).
[h] Dardenne (1978).
[i] Pimentel et al. (2001).

consisting of Fe-poor sphalerite with minor galena are tectonically imbricated with the willemite, metabasites, and dolostones. The willemite ore is commonly associated with specular hematite as well as lesser amounts of franklinite, smithsonite, zincite, barite, and quartz (Monteiro et al., 1999, 2007).

Fluid inclusion studies conducted on the willemite at Vazante by Dardenne and Freitas-Silva (1999) revealed salinities of 3–15 eq. wt.% NaCl and homogenization temperatures of 65–180 °C. Studies of sphalerite fluid inclusion conducted by Monteiro (2002) show salinities around 15–23 eq. wt.% NaCl and homogenization temperatures ranging from 201 to 232 °C. Monteiro et al. (1999) conducted sulfur and oxygen isotope studies and calculated the formation temperatures to be around 246–330 °C for sphalerite-galena, 263–294 °C for quartz–willemite, 206–254 °C for quartz–hematite, and 261 °C for quartz–siderite. The lower ranges of calculated temperatures are consistent with the sphalerite homogenization temperatures obtained by Monteiro (2002). Monteiro et al. (1999) and Appold and Monteiro (2009) proposed the formation of the Vazante deposit as being the result of mixing between a hot, saline, acidic, metalliferous fluid and cooler, oxidizing meteoric water. However, Monteiro et al. (1999) proposed that the metalliferous fluids were oxidizing and Appold and Monteiro (2009) suggested that they were reducing. The ore would then have precipitated out as a result of an increase in pH and possibly a small decrease in temperature (Appold and Monteiro, 2009).

4. The Northern Extension orebodies: Geology and mineralization

4.1. Geologic units

The Northern Extension mineralization is hosted by the Vazante Fault Zone that cuts through the Serra do Poço Verde and Morro do Calcário Formations of the Vazante Group and is truncated by a transposed fold contact with the phyllites from Serra do Garrote Formation (Fig. 3). Each of these formations has been metamorphosed to sub-greenschist facies.

In proximity to the zinc mineralized zones, the Serra do Garrote Formation (Fig. 4A) is comprised of a sedimentary marine sequence, with dark gray to black phyllites containing local zones of chlorite alteration, pyrite-rich boudins, and calcite veins. The Serra do Garrote has a tectonic contact with the overlying Serra do Poço Verde Formation.

The four members of the Serra Poço Verde Formation were identified during mapping and drill core logging. The Lower Morro do Pinheiro Member was not observed in outcrop but its surface location can be determined from the projection of drill logs. In drill cores, the unit is composed of gray to dark gray dolomite with algal layering and brecciated lenses (Fig. 4B). The contact between the Lower Morro do Pinheiro and underlying Serra do Garrote was not observed in these cores.

The Upper Morro do Pinheiro Member is composed of dark gray dolomite with bird's eye structures and some algal mat layering (Fig. 4C). A few meters of fine-grained black phyllites were also observed. According to Shinn (1968), the presence of bird's eye structures may indicate a supratidal to intertidal depositional environment. This member typically has carbonate filled tension fractures, silica alteration selvages, and occasionally dolomitic overgrowths with some veins containing pyrite and bitumen. It has a gradational contact with the Lower Pamplona Member.

The Lower Pamplona Member is comprised of pink to light gray dolomite, primarily dolarenite (Fig. 4D) and lesser dolorudite, intercalated with green to maroon phyllite (Fig. 4E). The dolomitic intervals of the Lower Pamplona contain algal mats and minor oncolites as well as vugs that may be filled in with recrystallized dolomite or chalcedony. The presence of algal mats and oncolites suggests a deposition in an intertidal to supratidal environment (Préat et al., 2010). The Lower Pamplona dolostone tends to be readily identifiable in the field, as it forms well indurated outcrops that weather to a beige or orange-brown color. Iron carbonate veinlets and silica-filled vugs are common throughout the dolostones in the Lower Pamplona. The phyllites exhibit clear north–south trending parasitic folds and crenulations, similar to those found in the Serra do Garrote Formation.

Formation	Member	Depositioinal Environment (thickness)	Description
Lapa	Serra da Lapa Velosinho	Rhythmites[1]	Black carbonaceous slate with dolomite lenses[1]
Morro do Calcário	Upper Pamplona	Supratidal facies Basal unit is storm beach facies (200-400 m)	Massive, dark gray dolarenite with stromatolites and minor black phyllites; Basal unit is dark, marroon siltstones[2]
Serra do Poço Verde	Middle Pamplona	Subtidal to intratidal (50-200 m)	Massive pink to gray dolostone with algal mats and stromatolites[1, 2]
	Lower Pamplona	Inter to supratidal facies (150-300 m)	Pink dolostone intercalated with maroon and green phyllites. Contains the hydrothermal breccia and pervasive hematite and ferroan dolomite alteration veinlets[2]
	Upper Morro do Pinheiro	Subtidal to intertdial facies (200-300 m)	Dark gray dolostone with bird's eyes and algal mats with thin layers of black phyllite near the base[2]
	Lower Morro do Pinheiro	Subtidal facies[2] (50-100 m)[1]	Light gray to pink dolostone with local intraformational breccias[1]
Serra do Garrote		Deep water, passive margin sediments (500+ m)	Dark grey phyllite, weathers to red and green. Contains localized zones of pyrite and calcite veins
Lagamar	Sumidouro	Intertdial facies	Gray limestone and dolostone with stromatolitic bioherm[1]
	Arrependido		Basal dolomitic breccia[1]
Rocinha		Rhythmites[1]	Rhythmites interbedded with phosphorite bearing slates[1]
Reteiro/ Santa Antônio do Bonito		Glacio-marrine[1]	Quartzite and diamictite with phyllitic intercalations Basal conglomerate[1]

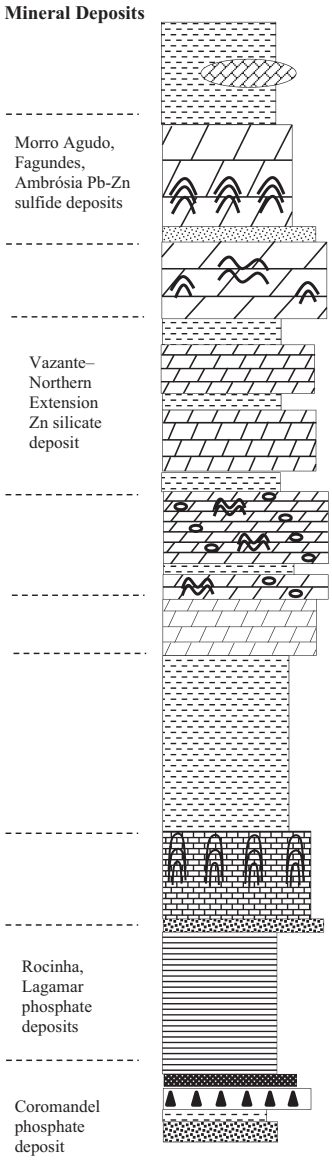

Fig. 2. Stratigraphic sequence of the Vazante region including the Northern Extension area. Modified from [1]Dardenne (2000), [2]Slezak (2012).

Iron carbonate and hematite hosted in veins and veinlets are common in all rock types of the Lower Pamplona Member.

The Middle Pamplona Member is comprised of a massive pink and gray dolostone (Fig. 4F) with moderate silica alteration in the form of veins and chalcedony-filled vugs that resemble those in the Lower Pamplona dolomites. However, dolostones in the Middle Pamplona Member are not interbedded with phyllites and contain some algal mat layering as well as stromatolites, indicative of a subtidal depositional environment as per Warren (2006) and Préat et al. (2010). Collapse breccias filled with carbonate cement and sulfides are also present in small occurrences.

The Upper Pamplona Member of the Morro do Calcário Formation is composed of light gray dolarenite with stromatolitic bioherms, indicative of subtidal environments according to Warren (2006) and Préat et al. (2010). Collapse breccias, such as those mentioned in the Middle Pamplona Member, are also found in the Upper Pamplona Member (Fig. 4G), though they are less common. The contact between the Morro do Calcário Formation and the Middle Pamplona Member is characterized by a dark, reddish-gray silty marker bed, which occurs in drill core throughout the Northern Extension region. This unit contains detrital zircons, which are currently being investigated for U–Pb dating.

4.2. Structures

The carbonate and clastic units in the Northern Extension deposit were deformed by compaction and developed a weak mineral grain alignment during the first deformation (D_1). The phyllitic units exhibit an S_1 cleavage that is subparallel to bedding (S_0). These S_0/S_1 surfaces are openly folded in the carbonate units and formed open to tight folds in the less competent phyllitic units of the Serra do Garrote Formation (Fig. 5A) and the Lower Pamplona Member during a second deformation event ($D_{2)}$. The fold axes have a trend and plunge of approximately 210° and 30° SE, respectively. This second deformational event generated a crenulation cleavage (S_2) that strikes SSW ranging from 200 to 225° with dips of 30° to 70° NW. This cleavage

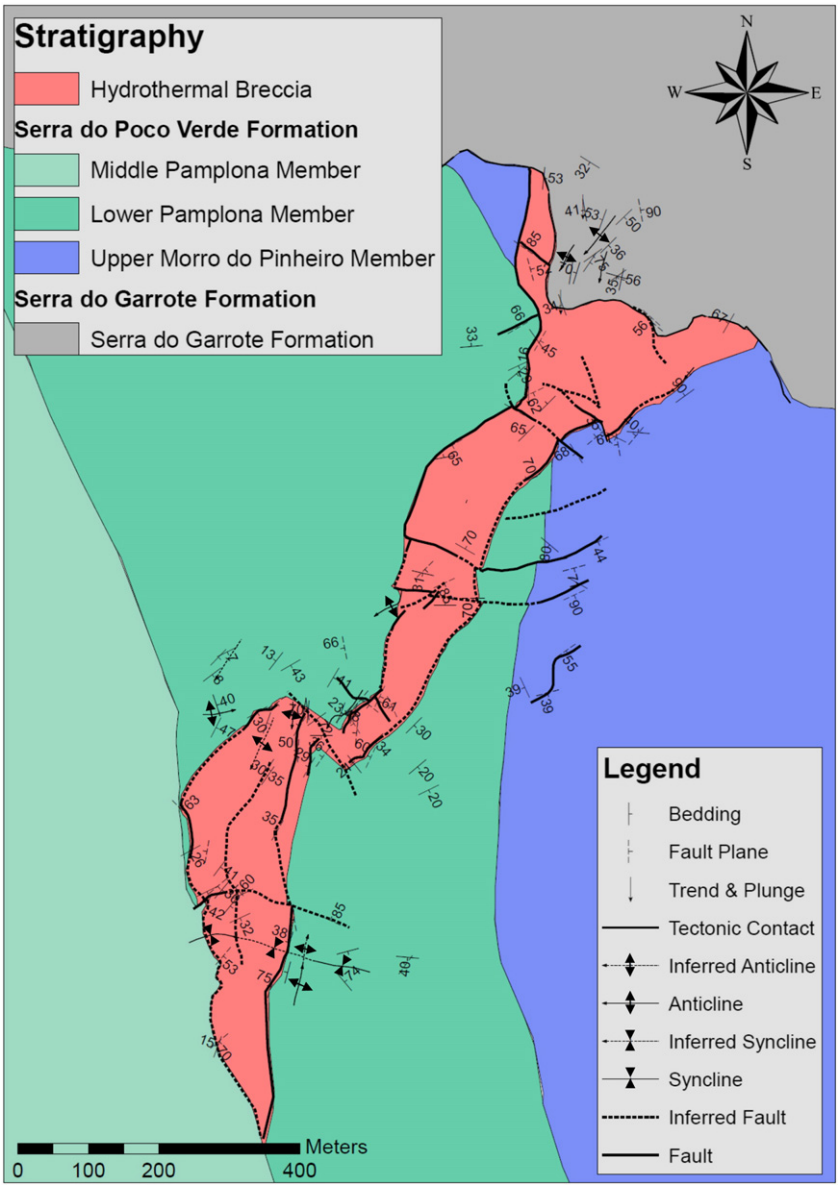

Fig. 3. Geological map of pits 5A, 6A, and 7A in the northernmost section of the Northern Extension. Modified from Votorantim base map; Slezak (2012).

is predominantly observed in the phyllites of the Serra do Garrote and Serra do Poço Verde formations (Fig. 5B) and was not observed in the carbonate units in the Northern Extension deposit.

The Northern Extension Fault Zone is controlled by two faults that have strikes and dips of 210°, 30° NW and 030°, 55° SE. The overall trend of the ore-bearing breccia zone is bounded by these faults. They are observed at the surface for about 600 m, are covered by lateritic soils in the southern limit of the North Zone property, and truncated in the north at the transposed fold contact of Serra do Poço Formation with the Serra do Garrote Formation. These faults appear to have been active for an extensive period of time, showing evidence of multiple motions as indicated by several sets of slicken lines as well as brecciation of multiple willemite ore phases. Regionally, these sets of NNE-trending faults are interpreted to have originated as normal faults created by extension during the initial rifting of the São Francisco Craton (Martins-Neto, 2009; Valeriano et al., 2008). Subsequent motion on these faults has not been clearly established. Valeriano et al. (2008) and Martins-Neto (2009) proposed that they were reactivated as oblique reverse faults during compression caused by the Brasiliano Orogeny. However, Rostirolla et al. (2002) interpreted the faults to be transverse and sinistral. Rigobello et al. (1988) and Dardenne (2000) reported the faults to be both sinistral and normal faults. Slickensides observed in this study indicate that the most recent movement was oblique-normal (Slezak, 2012).

The ore-bearing tectonic-hydrothermal breccias hosted in the fault zone do not cross-cut the transposed folded (D_2) contact with the Serra do Garrote Formation, suggesting that they were emplaced prior to or during early D_2 deformation. Moreover, the breccia trend is subparallel to axial planes that contain the β-axis (212 → 11) related to the D_2 folding event (Fig. 6A and B), supporting the interpretation that the breccia formed in the early stages of the D_2 folding event.

Late sinistral and dextral transverse faults (with strikes ranging from 065° to 170° dipping 30°–70° SW/SE: Fig. 6B) cut and displace the major fault structures bounding the tectonic-hydrothermal breccia by several meters as well as the contact with the Serra do Garrote Formation and the large anticline found in the northern pit wall of

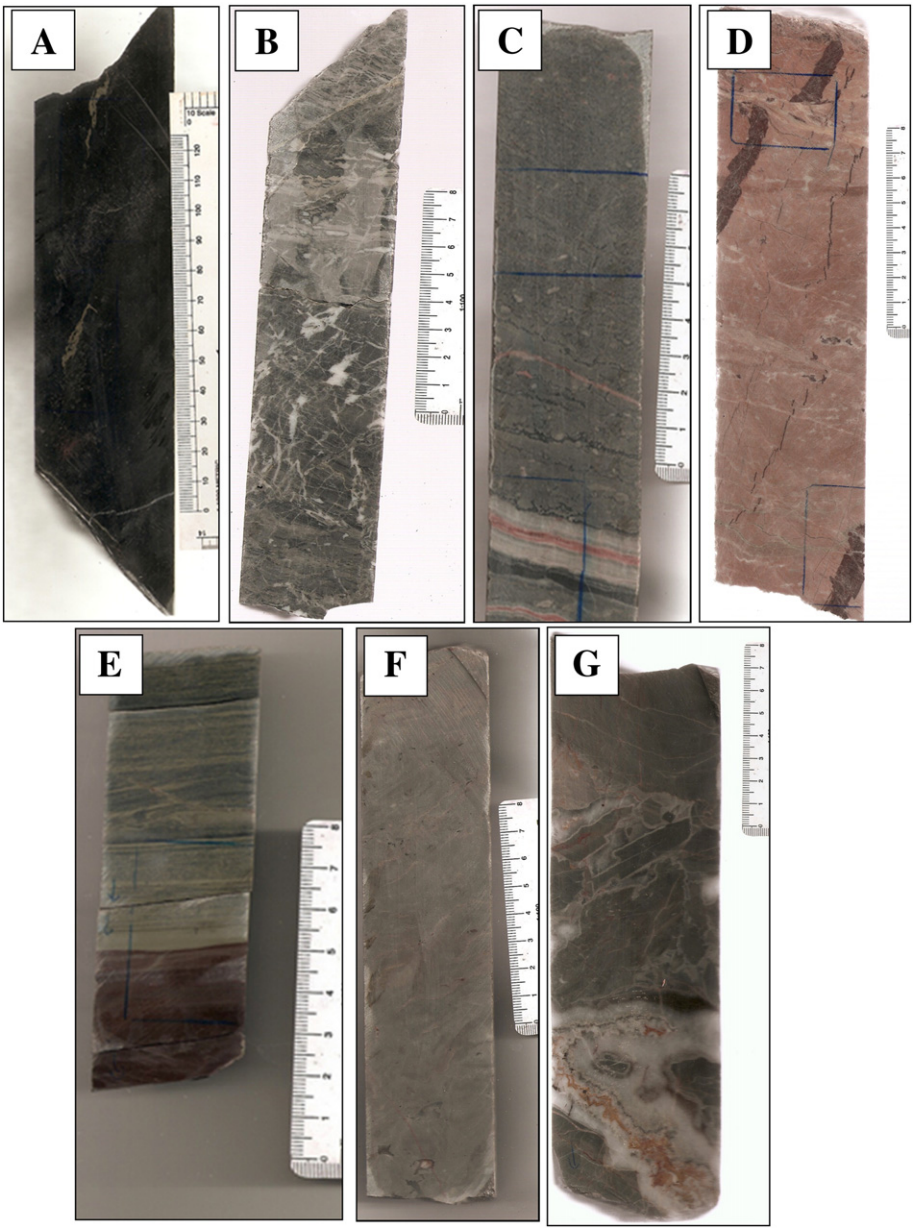

Fig. 4. Drill core samples of the geological units in the Northern Extension. A) Black phyllites with pyrite veinlets typical of the Serra do Garrote Formation (VZMSF 032 at 199 m). B) Gray crackle breccia of the Lower Morro do Pinheiro member. The fragments contain stromatolites and the fractures are filled with carbonate cement (VZMIF 004 at 408 m). C) Dark gray dolostone with bird's eyes and algal layering cross-cut by iron carbonate alteration veins in the Upper Morro do Pinheiro member (VZMIF 129 at 247 m). D) Massive pink dolostone that characterizes the Lower Pamplona cut by iron carbonate veins (VZMIF 122 at 94 m). E) Green and maroon phyllites from the Lower Pamplona member (MASA 124 at 267 m). These phyllitic layers are typically intercalated with the previously mentioned pink dolostone. F) Massive light gray dolostone of the Middle Pamplona Member (VZMIF 141 at 18 m). G) Gray dolostone of the Morro do Calcário Formation (Upper Pamplona Member) with local dissolution-collapse breccia with dolomite and siderite cement (VZMIF 124 at 42 m).

pit 7A. Most of the supergene calamine ore is associated with these faults. Small NW–SE trending joints also cross-cut the bounding faults of the tectonic-hydrothermal breccia as well as the transverse faults.

5. Analytical methods

Following the detailed mapping, logging, and sampling, polished thin section studies were completed in order to establish paragenetic relationships for ninety-nine representative samples. An FEI MLA 650 FEG-ESEM was used to verify the identification of less prevalent minerals in the samples and evaluate the variation in major elements of carbonate and willemite. The samples were not carbon coated and were analyzed under low vacuum pressure at 20.00 kV. Quantax energy dispersive X-ray spectrometer (EDS) readings were used to identify qualitative information about unknown minerals.

Electron microprobe analysis was completed at the New Mexico Bureau of Mines and Mineral Resources at New Mexico Tech. The analyses were completed using a Cameca SX-100 electron microprobe with three wavelength dispersive electrometers with secondary electron and high-speed backscattered electron detectors. A beam current of 20 nA was used for willemite and sphalerite, and reduced to 10 nA for carbonate analysis. The operating conditions, count times, and standards can be found in Slezak (2012). The purpose of the microprobe study was to determine the chemical variations within the willemite generations and various types of carbonate alteration (Appendix A).

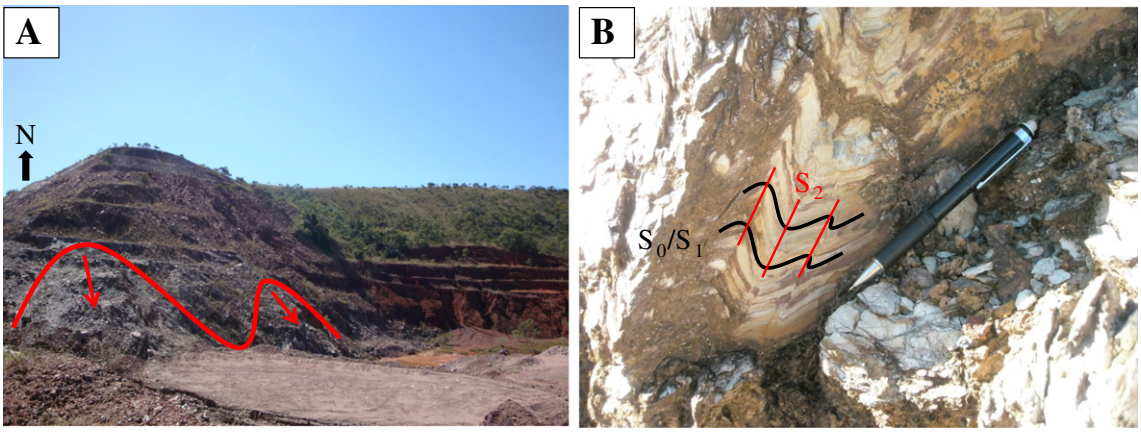

Fig. 5. A) Photograph looking to the northeast showing the plunging antiform–synform complex in the northern wall of pit 7A in the Serra do Garrote Fm. B) S_0 compositional layering with S_1 cleavage and S_2 crenulations found in phyllitic units in the Lower Pamplona Member.

Whole rock analyses of samples from each unit were conducted in order to determine the geochemical signatures related to the various styles of mineralization and alteration, as well as the gains and losses involved in the alteration process. The geochemical analyses were carried out by the ALS Laboratory Group, Sudbury, Ontario on 74 samples including the least altered and most representative samples of each of the local geologic units, the non-ore breccias, and the willemite ore samples. They were prepared using 4-acid (nitric, perchloric, hydroflouric and hydrochloric acids) digestion and then analyzed for 49 elements by inductively coupled plasma mass spectrometry (ICP-MS). This method was chosen against aqua regia because of its ability to digest both base metals and silicates due to the significance of willemite in this study. Additional analyses were conducted using alternative methods for selected elements and major oxides to account for possible interferences, losses in volatile elements (e.g. Hg), and analyses of refractory phases. The element As, in addition to samples containing greater than 100 ppm Ag and greater than 10,000 ppm Pb, were prepared using 4-acid digestion and analyzed using inductively coupled plasma absorption emission spectrometry (ICP-AES) to eliminate interferences and increase the upper detection limits. Mercury was analyzed by 4-acid digestion with trace vapor/atomic absorption spectrometry (AAS). Samples containing more than 10,000 ppm Zn were analyzed by titration. A subset of 39 samples was analyzed for whole rock geochemistry using X-ray fluorescence, to determine the amount of the major oxides. However, this combination of methods may not have allowed for very effective analyses of volatile elements such as Sb and Ge or some trace elements in very refractory phases. The full geochemical results can be found in Slezak (2012).

Major and trace elements selected from the four types of tectonic–hydrothermal breccias and their host rocks (Appendix B) were plotted in box and whiskers diagrams using ioGAS to evaluate their variation among rock types. Furthermore, isocon diagrams based on studies by Grant (1986) and Grant (2005) were constructed to identify and compare the elemental enrichment and depletion of selected elements among the various breccia types and least altered host rocks (e.g., least altered dolostone was plotted against type 1 breccia, and the latter was potted against type 2 breccia, etc.). Silica was plotted as SiO_2 based on the XRF data gathered from the breccia samples. This approach does not allow for quantitative mass balance calculations due to

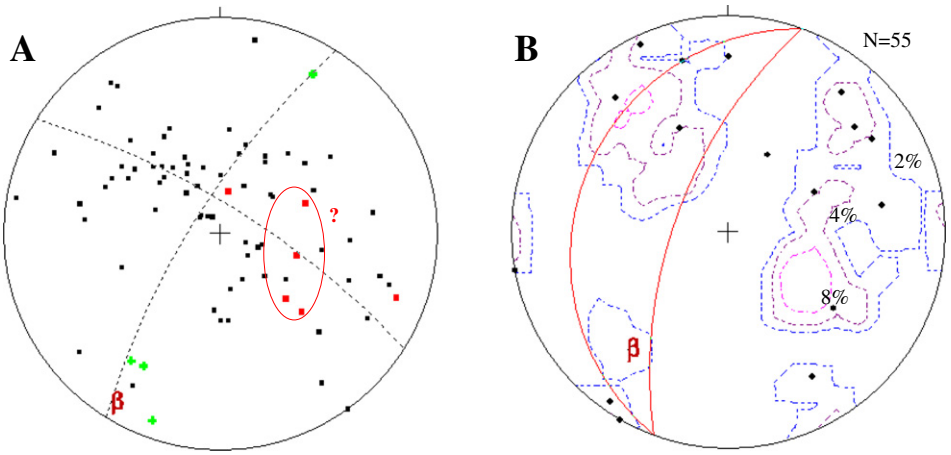

Fig. 6. A) Plots of the poles of S_0/S_1 compositional layering/foliation in black, S_2 crenulation cleavage in red, trend and plunges of major fold axes in green, and the average fold axis is denoted by the β-axis and plane of 212°, 79° NW. The circled red squares represent S_2 cleavages from a fault block, indicating that they were transposed by the fault. B) Plots of the poles of the conjugate fault planes bounding the tectonic–hydrothermal breccia are outlined in blues, purples, and pinks (from lowest to highest concentration of points). In black are fault plane poles to the later E–W transverse faults. Red solid lines represent the average strike of the tectonic–hydrothermal breccia with its ranges in dip.

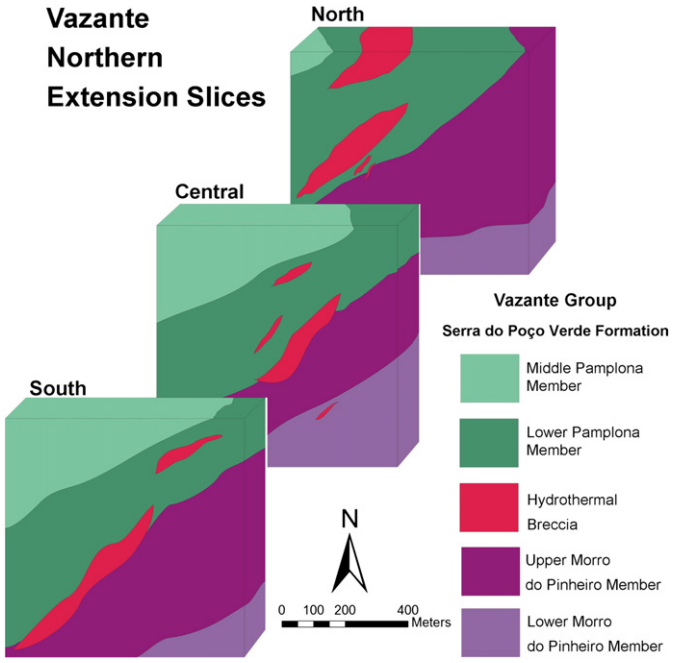

Fig. 7. Block diagram of the Northern Extension depicting the morphology of the tectonic–hydrothermal breccias and host rocks along strike. The Northern Extension orebodies are exposed at surface as represented by the northern blocks.

brecciation and infilling with breccia matrix and veins, but it permits to evaluate qualitatively which elements were mostly introduced during the various breccia stages.

The elements were scaled in order to better represent the wide range of abundances (0.1 ppm to 50%). The immobile elements necessary for the isocon line were determined to be Ce, La, Sc, Ti, and Y based on their high correlation coefficients to each other (>0.9) and because they are commonly immobile in sedimentary and low temperature conditions (Bhatia and Crook, 1986). The unscaled locations of these immobile elements were used to calculate the isocon lines on the plots.

6. North Extension tectonic–hydrothermal breccias

6.1. Major breccia types

The Northern Extension ore zone is comprised mainly of willemite (in variable amounts reaching up to 40%) and specular hematite (varying from 1% to 50%) with minor amounts of franklinite. These ore zones form discontinuous lenses (tens of meters in length and width) within laterally and vertically discontinuous tectonic–hydrothermal breccias (Fig. 7), which vary greatly in thickness from a few meters to nearly 100 m. The tectonic–hydrothermal breccia lenses within the fault zone plunge gently to the south. The fault zone has been reactivated during the evolution of the deposit and may have served as the main conduit for the hydrothermal fluids, as it hosts a variety of hydrothermal breccias.

Four main types of breccias have been identified based on their overall composition and relative position to the ore lenses. Type 1 breccia is the least altered and the most distal from the ore breccias (referred to as type 4 breccia). Breccia types 2 and 3 occur spatially between breccias 1 and 4. All the breccia types are composed mainly of gray, pink, red, and white dolostone fragments and some with minor phyllite fragments from the Lower Pamplona Member. Many of the clasts are rimmed by recrystallized red and/or white dolomite. The cement between clasts is composed of various proportions of ferroan dolomite, zincian dolomite, quartz, and hematite, depending on the breccia type.

Type 1 breccia: Contains angular, cobble-sized clasts of gray to white dolostone with red and white dolomite cement. Both the clasts and cement are cross-cut by ferroan dolomite veinlets (Fig. 8A). These breccias are commonly located between the unbrecciated host rocks and the intensively altered ferroan dolomite breccias (type 2) and are interpreted to have formed during

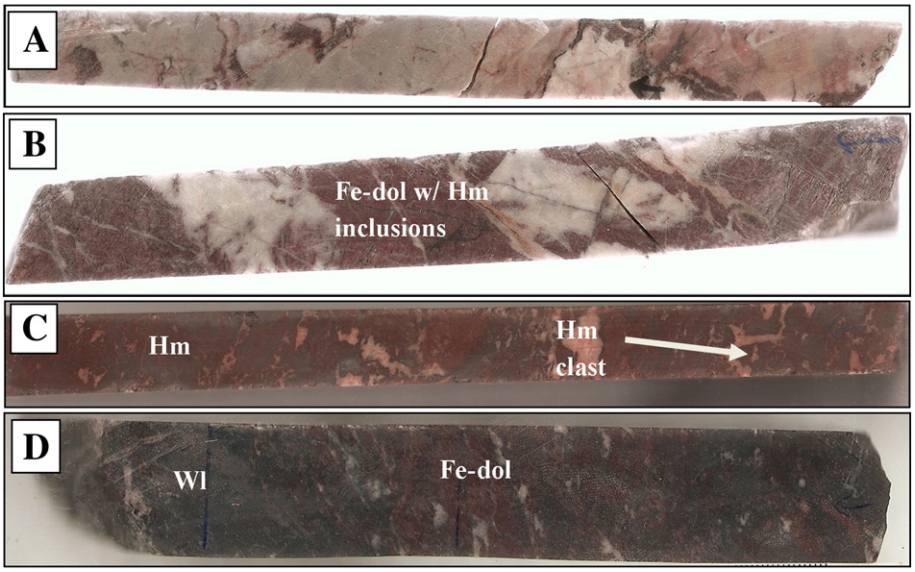

Fig. 8. Drill core samples illustrating the characteristics of the various types of hydrothermal breccias: A) Type 1 — Light-colored, weakly brecciated dolostone with Fe, Zn-dolomite veinlets (MASA 124 at 256 m). B) Type 2 — Strong hydrothermal Fe, Zn-dolomite alteration in dolostone. The reddish color is caused by small hematite inclusions and hematite staining within the ferroan dolomite (VZMIF 043 at 232 m). C) Type 3 — Hematite-rich breccia (>40% Fe). The hematite is present as clasts and more ductile shears in this sample (VZMIF 125 at 55 m). D) Type 4 — Main ore breccia with willemite and red, ferroan dolomite with hematite inclusions (VZMIF 101 at 144 m).

the initial phases of brecciation. Dolomites from veins and veinlets have an average of 1.29 wt.% FeO and 0.13 wt.% ZnO (Table A1). The zinc content is lower than in the dolomite in the breccias proximal to the ore. Red hydrothermal dolomite typically contains hematite inclusions, although high iron contents are observed in white hydrothermal dolomite as well.

Type 2 breccia: Contains angular dolomite clasts (1 to 100 cm in diameter) that are strongly altered to red ferroan dolomite. Reddish orange and white ferroan–zincian dolomite veinlets (0.3 to 2 cm wide) and dark red, hematite-stained alteration veinlets are very abundant (Fig. 8B). The ferroan and zincian dolomites are comprised of 1.5 to 3.3 wt.% FeO and 0.3 to 1.25 wt.% ZnO, respectively (Table A1). Sparry, zoned, euhedral dolomite occurs in the center of the veins and hematite is found mainly on the vein margins or as small inclusions within the red dolomite. These breccias are generally proximal to the type 3 (hematite) breccias and mineralized type 4 (willemite). They are distinguished from the type 1 breccia by more intense brecciation and the occurrence of Fe-carbonate as both replacement of the dolomite clasts and as vein infill.

Type 3 breccia (*hematite-rich breccia*): Deep red colored breccia with irregularly shaped clasts that are composed predominantly of hematite with traces of willemite. White dolomite cement is also present in small amounts (Fig. 8C). These breccias are commonly found in the margins of the type 4 breccia or as isolated breccia zones (1–3 m wide) in the fault zone. Hematite (40–75%) fills embayments in carbonates in the cement and clasts and in veinlets cross-cutting the first two breccia types, which indicates that these hematite-rich breccias formed after the major Fe–dolomite hydrothermal episode.

Type 4 breccia (*willemite ore breccia*): The ore breccias are commonly found in the core of the tectonic–hydrothermal breccia structure, mantled by and inter-fingered with type 3 breccias. The type 4 breccia (Fig. 8D) comprises willemite and hematite up to 10–50% and 5–20% of the breccia, respectively, and minor amounts of franklinite, ferroan (~1.99 wt.% FeO) and zincian

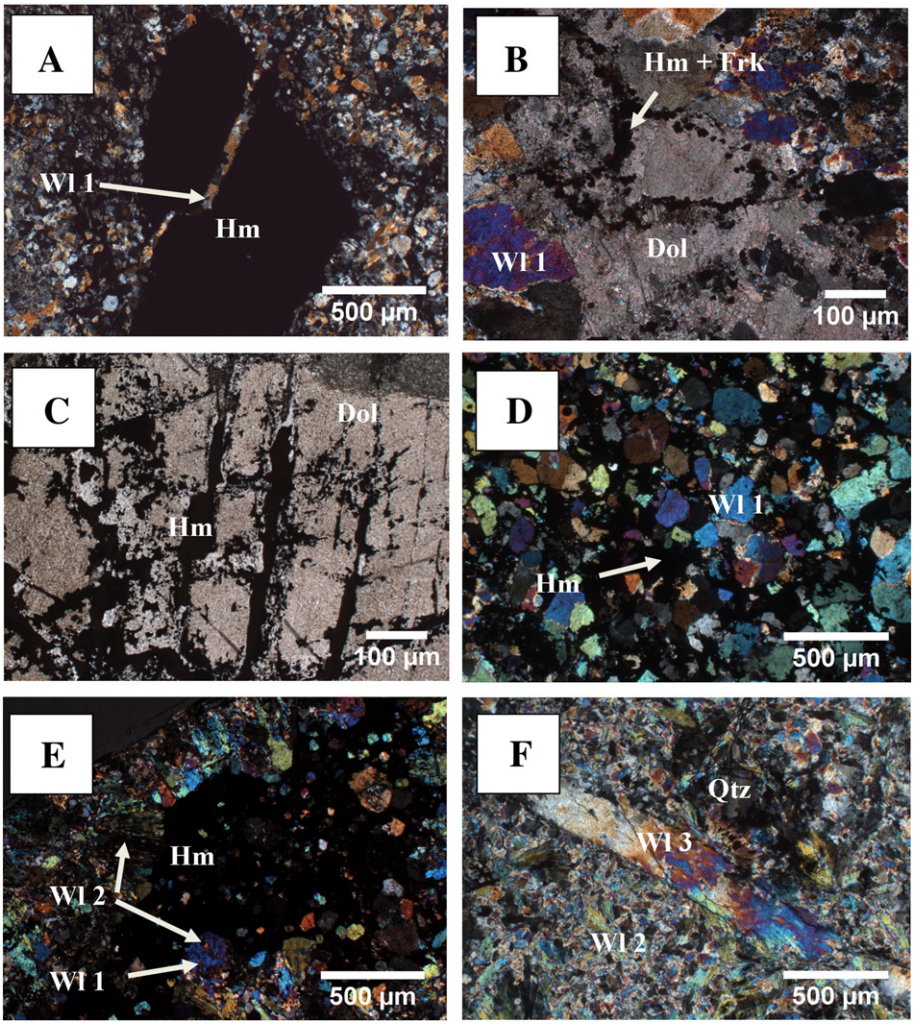

Fig. 9. Photomicrographs showing the minerals and their textural relationships in the Type 4 Breccia. B) Sample 101-138, subhedral to euhedral, generation 1 willemite with hematite and franklinite replacing dolomite (under incident light and crossed polars). C) Sample 105-113A, hematite replacing dolomite along cleavage planes (under incident light). D) Sample 106-122, euhedral generation 1 in a hematite matrix (under incident light and crossed polars). E) Sample 123-73, lath-shaped generation 2 willemite overgrowing subhedral generation 1 willemite. Hematite is replacing both willemite generations (under incident light and crossed polars). F) Sample 060-136B, a small, fibrous, generation 3 willemite veinlet cross-cutting lath shaped generation 2 willemite (under incident light and crossed polars). Wl = Willemite, Frk = Franklinite, Hm = Hematite. Dol = Dolomite. Qtz = Quartz.

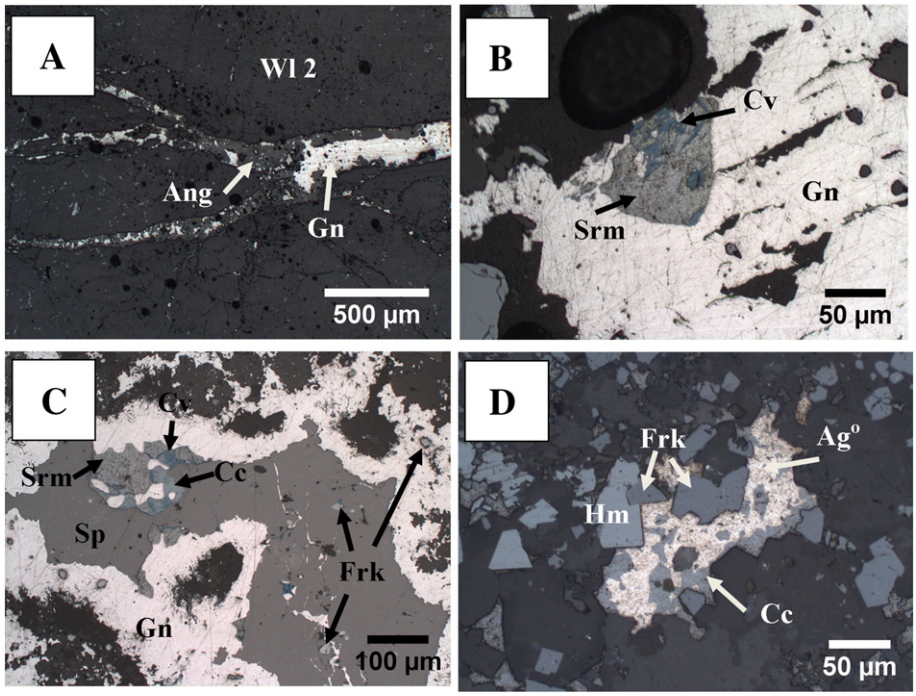

Fig. 10. Photomicrographs showing the minerals and their textural relationships in the Type 4 Breccia. A) Sample 060-136A, galena (partially replaced by anglesite) veinlets cross cutting generation 2 willemite (under reflected light). B) Sample 060-136B stromeyerite being replaced by covellite. Both minerals are overgrowing galena. C) Sample 060-136A, sphalerite–galena veinlets with stromeyerite altering to covellite and chalcocite (reflected light). D) Sample 012-347A, euhedral hematite blades surrounded by Ag-bearing chalcocite, which is being overgrown by Ag^o (under reflected light). Sp = Sphalerite, Gn = Galena, Ang = Anglesite, Wl = Willemite, Frk = Franklinite, Srm = Stromeyerite, Cc = Chalcocite. Cv = Covellite, Hm = Hematite, Ag^o = Native Silver.

(~2.65 wt.% ZnO) dolomite (Table A1) and quartz. However, the presence of hematite is not ubiquitous throughout the willemite ore zones. Type 4 breccia is locally cut by small sulfide veinlets, and its mineralogy and textural relationships are described in detail below and illustrated in Figs. 9 and 10.

6.2. Mineralogy and paragenesis of the ore breccia (type 4)

Willemite (0.1 to 0.75 mm) occurs as hexagonal crystal masses replacing dolostone clasts (Fig. 9A, B, and D). It also occurs as lath-shaped crystals, and small, discontinuous veins that cut across many clasts in the breccia zone. It locally replaced carbonates as

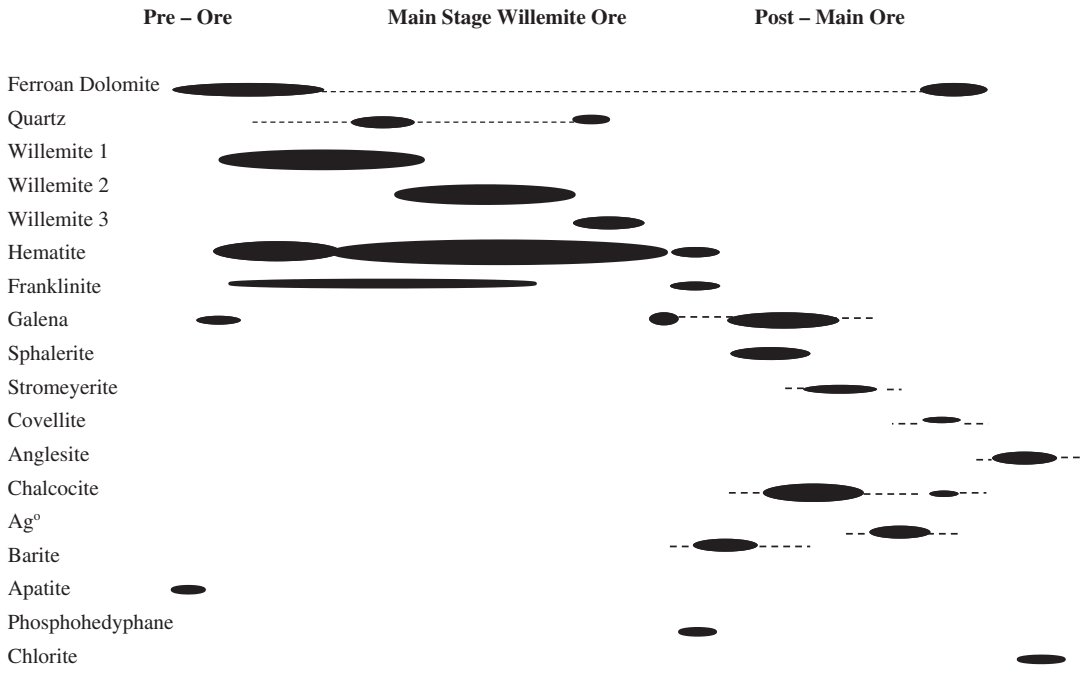

Fig. 11. Paragenetic sequence of the zinc silicate mineralized zone in the Northern Extension orebodies.

well as quartz clasts and crystals. The lath-shaped willemite overgrew the earliest, hexagonal willemite (Fig. 9E). The small (100–300 μm wide), discontinuous willemite veins cut through both the fibrous laths (Fig. 9F) and the hexagonal willemite, indicating that they formed during the last stages of mineralization. The willemite composition varies little throughout all three generations. Its average FeO content is 0.4 wt.% (Table A2). Hematite (0.01 to 1 mm) commonly occurs as either aggregates of fine-grained blades filling in spaces between clasts (Fig. 9B), or disseminated, larger crystals replacing early willemite and carbonates (Fig. 9C and D). Some hematite clasts are cut by willemite as well (Fig. 9A). Euhedral laths are also found included in willemite and in the margins of late sulfide veins (Fig. 10D).

Franklinite is most commonly found as small octahedral inclusions associated with hematite (Fig. 9B) in willemite-rich domains. It is also found as inclusions in willemite and dolomite, as very small (1 to 10 μm) disseminated crystals in the breccia matrix, and spatially associated with hematite in the margins of the sulfide veinlets (Fig. 10C and D).

Small, 10–50 mm, galena-rich veinlets cross-cut the main willemite ore (type 4 breccia) and contain small amounts of sphalerite, stromeyerite ($Cu_{1-x}Ag_{1-x}S$), chalcocite, and covellite (Fig. 10A–C). Galena is massive within the veinlets and is altered to anglesite ($PbSO_4$) on the veinlet margins (Fig. 9A). Sphalerite in these veinlets (Table A3) is cadmium-rich (2.88–3.10 wt.%) and iron-poor (0.01–0.02 wt.%), similar to the sphalerite reported by Monteiro et al. (2006) in the Vazante deposit, and is found as irregular crystals within galena. Stromeyerite forms irregular, disseminated crystals, generally alters to bladed covellite, and more rarely to chalcocite (Fig. 10B and C).

Silver-bearing sulfide veinlets (10–100 mm wide) cross-cut willemite ore in one drill hole and are similar in morphology to galena veinlets described above. The veinlets are primarily composed of chalcocite, native silver, stromeyerite, franklinite, hematite, and minor galena (Fig. 10D). Barite and phosphohedyphane ($Ca_2Pb_3[PO_4]_3Cl$) occur in small amounts as disseminated anhedral to subhedral crystals ranging in size from 20 to 50 μm. In backscattered electronic images, chalcocite shows a complex texture of light and dark gray zoning with the lighter gray sections containing 1.1–1.5% silver, and the darker gray sections containing trace amounts or no silver (Slezak, 2012).

Based on the field and textural relationships, the interpreted paragenesis for the Northern Extension mineralization is presented in Fig. 11 and summarized here:

Stage 1 (pre-ore): Early brecciation of the Serra do Poço Verde dolostones and precipitation of Fe-bearing dolomite cement in between dolostone clasts (types 1 and 2 breccias).

Stage 2 (syn-main ore): Formation of the hematite-rich type 3 breccia and the willemite-rich type 4 breccia with multiple episodes of precipitation of willemite, hematite, franklinite, ferroan and zincian

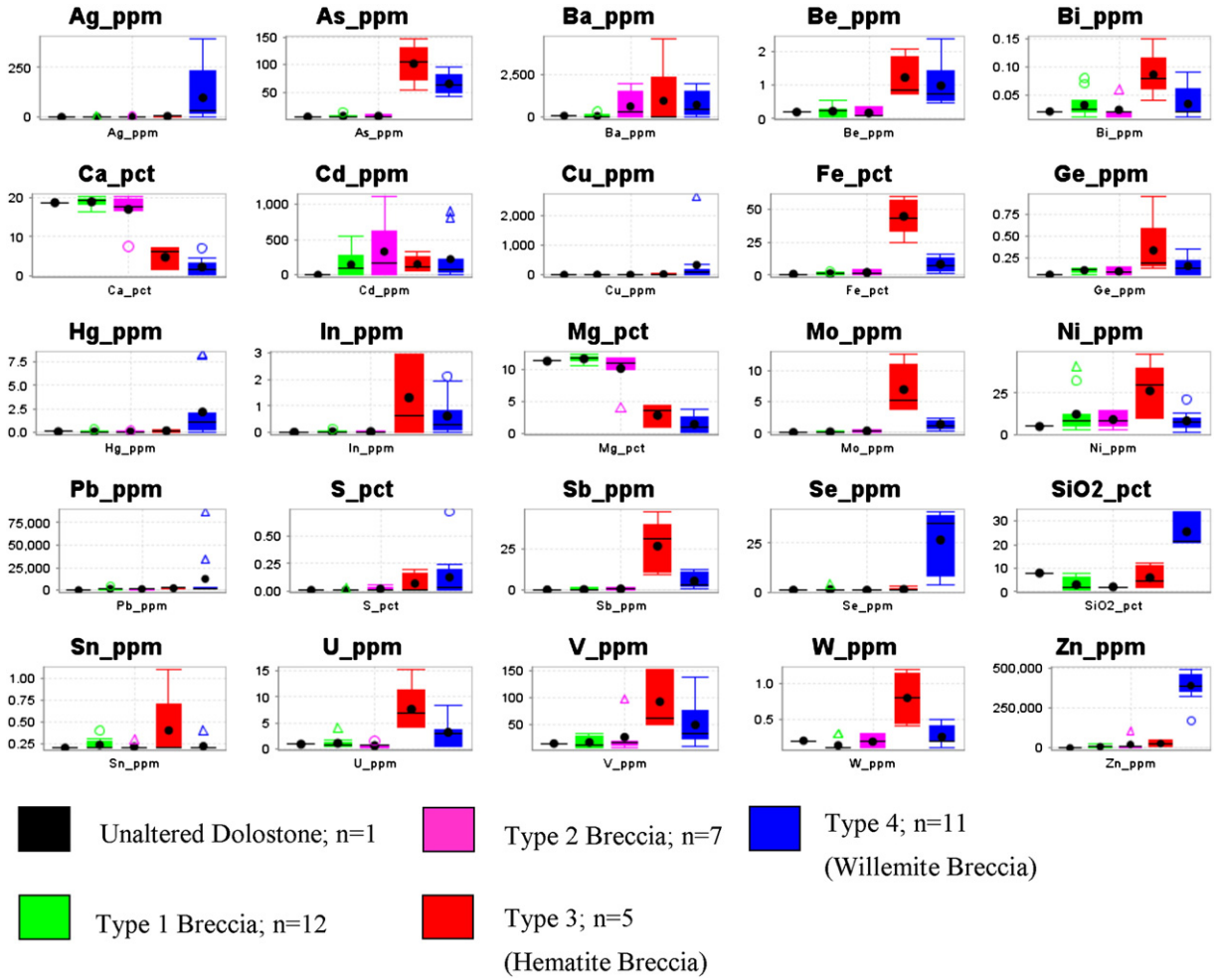

Fig. 12. Box and whisker plots showing the variation in composition of the major ore-related elements of the least altered Lower Pamplona Member (black), type 1 breccia (green), type 2 breccia (pink), type 3 breccia (red), and type 4 breccia (blue).

dolomites that filled fractures and replaced the earlier-formed breccia dolostone clasts and matrix.

Stage 3: (post-main ore): Subsequent to the main ore stage, the Pb-rich and Ag-rich sulfide veinlets formed and cross-cut the main ore stage minerals.

7. Lithogeochemistry of the main breccia types

Box and whiskers plots for selected elements related to the ore-forming process (Fig. 12) show that the variations among the compositions of the least altered samples and type 1 and 2 breccias are minor; however, type 3 and 4 breccias show significant variations when compared to the least altered host rock, type 1 and type 2 breccias. Type 3 and 4 breccias yielded the highest averages in As, Ba, Be, Bi, Fe, Ge, In, Mo, Ni, Sb, U, V, and W, with type 3 breccia being the most enriched in these elements. Type 4 breccia has significantly higher average concentrations of Ag, Cu, Hg, Pb, S, Se, SiO_2, and Zn compared to the unaltered carbonate host rocks. Type 3 and 4 breccias show an increase in the element concentrations of Ag, Cu, Pb, and Zn as well as a decrease in the concentration of Ca and Mg, due, in part, to the replacement of the carbonate minerals and, in part, to the deposition of hematite and willemite filling fractures in the breccias.

Figs. 1–3A, B, C and D are isocon plots that represent the evolution of comparative element gains and losses of a sample relative to a less altered sample. The reference isocon line was defined by the line of best fit through the immobile elements Ce, La, Sc, Ti, and Y. The isocon plot illustrating the unaltered Lower Pamplona dolostone with the type 1 breccia (Fig. 13A) reveals that this breccia is enriched in a variety of elements including Ag, As, Bi, Cd, Co, Cu, Fe, In, Mn, Mo, Ni, P, Pb, Sb, and Zn. The type 1 breccia is depleted in K, Rb, and SiO_2. When the type 2 breccia is compared to type 1 breccia (Fig. 13B), it can be seen that the type 2 breccia is slightly enriched in the same suite of elements as type 1 breccia and greatly enriched in Zn and Fe. The type 3 breccia is enriched in Ag, As, Ba, Bi, Cd, Co, Cu, Fe, Ga, Ge, Hg, In, Mo, Ni, Pb, Sb, Se, SiO_2, U, V, and Zn but depleted in Ca, K, Mg, and Rb compared to the type 2 breccia (Fig. 13C). The type 4 breccia is enriched in Ag, Cd, Cu, Hg, Pb, S, Se, SiO_2, Sr, and Zn relative to the type 3 breccia. Both the type 3 and 4 breccias showed increased concentrations of Ag, Cd, Cu, Hg, Pb, Se, SiO_2, and Zn (Fig. 13D). Many of the elements previously enriched in the other breccias fall on the isocon and show no change or are slightly depleted compared to the Type 3 breccia. Although quantitative mass balance cannot be performed due to mass and volume gain during breccia matrix and veinlet infilling, which are concomitant with clast and matrix replacement, the qualitative relationships identified above are very consistent with mineral and mineral chemistry data presented in the previous sections and discussed below.

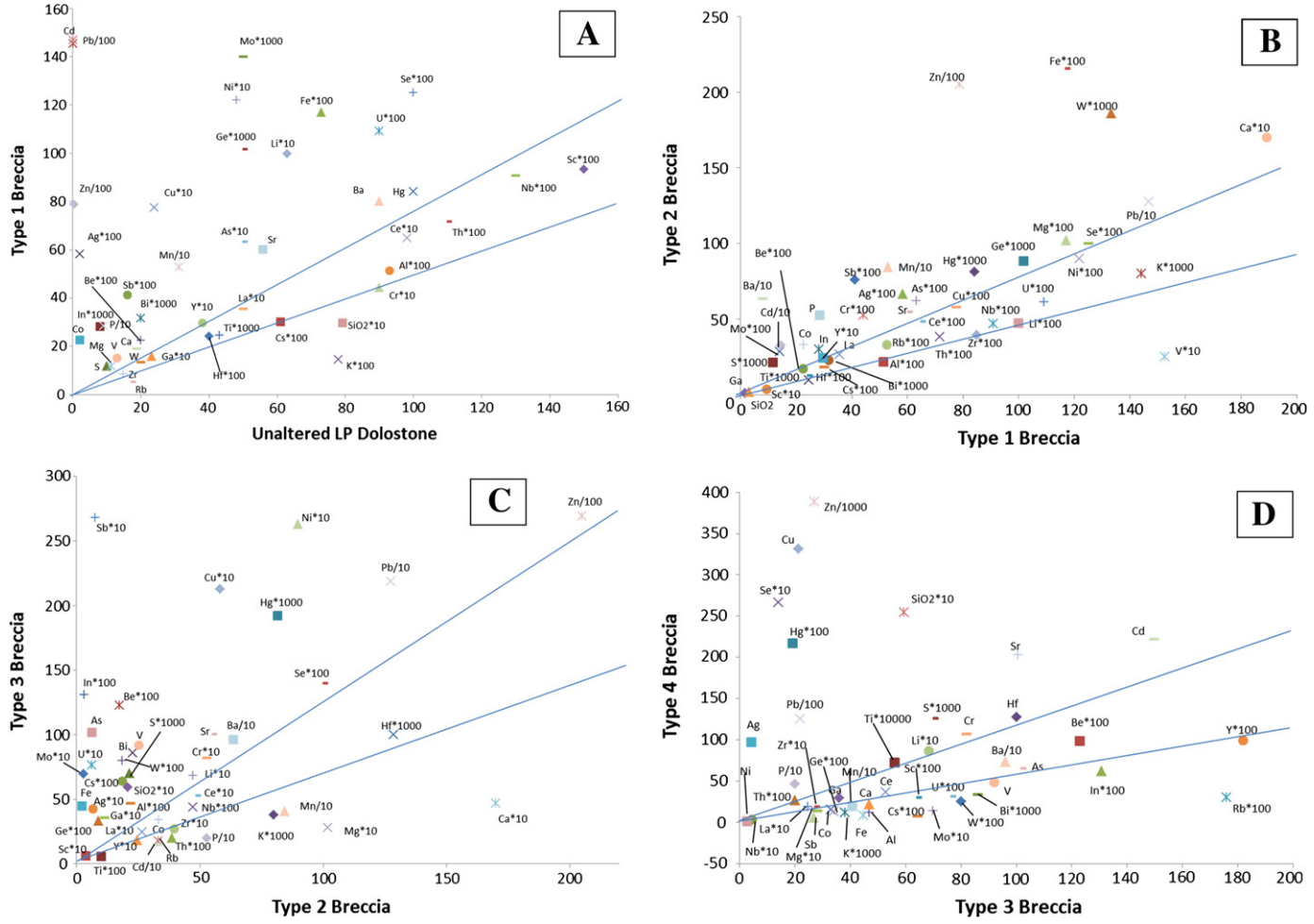

Fig. 13. Isocon plot in ppm with factor-corrected data of A) type 1 breccia vs. unaltered dolostone from the Lower Pamplona Member, B) type 1 breccia vs. type 2 breccia, C) type 2 breccia vs. type 3 breccia, D) type 3 (hematite) breccia vs. type 4 (willemite) breccia showing the gains and losses during the evolution of the hydrothermal system (see text for further explanation).
Lithogeochemical data from Slezak (2012).

8. Discussion

8.1. Evolution of the Northern Extension system

Subsequent to deposition and dolomitization of the passive margin carbonates in the Serra do Poço Verde Formation after c.a. 900–1000 Ma, tectonism began with the onset of the Brasiliano Orogeny around 850 Ma (Martins-Neto, 2009; Misi et al, 2005). Compaction and/or deformation related to the beginning of the Brasiliano Orogeny (D_1) created a regional foliation (S_1) subparallel to bedding (S_0) within the phyllite units of the Vazante Group. Continued deformation (D_2) of the region folded the S_0/S_1 foliation, resulting in an S_2 crenulation cleavage, regional folds, and the NE-striking conjugate faults of the Vazante-Northern Extension. These features were

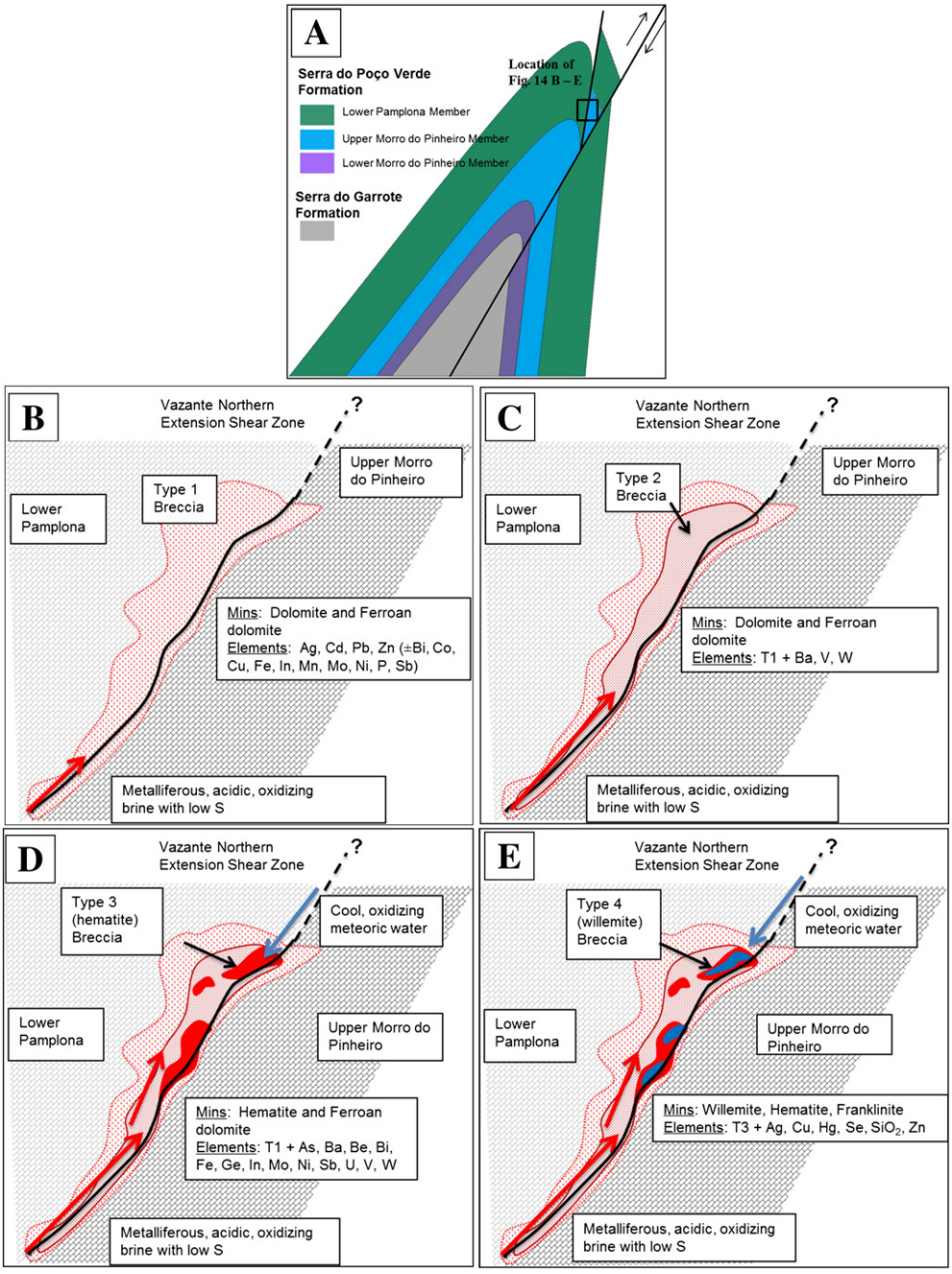

Fig. 14. Genetic model for the Vazante Northern Extension Deposit. Note: T1, T2, and T3 stand for type 1, type 2, and type 3 breccia, respectively. A) The schematic diagram of the Serro do Poço Verde and Serra do Garrote formations represents a possible regional tectonic setting and location for the Vazante Northern Extension ore bodies that would allow for fluid percolation through faults according to Cooley et al. (2011a,b). B) Initial brecciation from tectonism and hydraulic pumping of the dolomites with of basinal brine, forming type 1 Breccia. C) Continued brecciation from hydraulic pumping and fluid interaction and hydrothermal alteration, forming type 2 breccia. D) Mixing of cool, oxidizing, meteoric water with basinal brine, forming type 3 breccia rich in hematite and ore-related elements (red). E) Further mixing of cool, oxidizing, meteoric water with basinal brine, resulting in dilution and pH increase, forming type 4 willemite ore breccia (blue).

most likely coeval with the formation of the thin-skinned nappes and low-grade metamorphism as described by Dardenne (2000), Valeriano et al. (2008), and Martins-Neto (2009). This geometry is similar to that described in the Canadian Cordillera foothills, where the propagation of detachment faults caused flexural folding (Fig. 14A: Cooley et al., 2011a). These structures may have created the ideal setting to focus the flow of deeper hydrothermal fluids in the fault zones and along the contacts between rocks with distinct rheological behavior (such as dolomites and phyllites) and to allow the percolation of meteoric fluids in the normal faults (Fig. 14A: Cooley et al., 2011a,b).

The hydrothermal metalliferous fluids associated with Vazante-North Extension deposit were most likely saline in which zinc was transported as $ZnCl_4^{2-}$ and iron as $FeCl_3$ according to Riveros and Dutrizac (1997) and Brugger et al. (2003), and acidic enough to dissolve the dolomitic host rocks. These hydrothermal fluids that circulated in the sedimentary sequence would have moved through the Northern Extension Fault Zone, fracturing and dissolving the Lower Pamplona carbonates, creating the type 1 breccia (Fig. 14B). The type 1 breccia is characterized by weak brecciation; Fe-dolomite alteration and veinlets; substantial enrichments in Ag, Cd, Pb, Zn; and moderate enrichments in Bi, Co, Cu, Fe, In, Mn, Mo, Ni, P, and Sb. Enduring basinal fluid flow caused further brecciation and alteration, creating the strongly Fe-dolomite altered type 2 breccia (Fig. 14C), which exhibits a similar geochemical signature to the type 1 breccia. These basinal fluids may have been oxidizing, as most of these elements are more soluble under oxidizing conditions. This interpretation is in agreement with the model proposed by Monteiro et al. (2007) based on mineralogical and geochemical evidence and in disagreement with Appold and Monteiro (2009), who based on numerical modeling, proposed that the metalliferous brine was reducing. After the formation of type 2 breccia, there was a substantial change in the hydrothermal fluid conditions as indicated by the observations that (a) the hydrothermal breccias changed from clastic dolostone and carbonate cement-dominated breccias to hematite and willemite breccias, in part formed by replacement of the dolostone clasts and carbonate matrix, and in part by the emplacement of veins, and (b) the substantial increase in concentrations of As, Ba, Be, Bi, Fe, Ga, Ge, Hg, In, Mo, Ni, Pb, Se, SiO_2, and Zn. These major changes in mineralogy and abundance of ore-related elements could be explained by mixing between the basinal brine and the more oxidizing fluids, probably of meteoric origin (Fig. 14D). These changes would have generated the conditions necessary to stabilize hematite. A possible reaction for the formation of hematite from Fe-bearing carbonates is:

$$8Ca(Mg_{0.5},Fe_{0.5})(CO_3)_{2(solid)} + 12FeCl_{3(aq)} + 24H^{+}_{(aq)} + 6H_2O + O_2 = 8Fe_2O_{3(solid)} + 36HCl_{(aq)} + 8Ca^{+2}_{(aq)} + 4Mg^{+2}_{(aq)} + 16CO_{2(gas)}. \quad (1)$$

As the system became cooler, more dilute, or more basic, the conditions became favorable for the precipitation of willemite (Fig. 14E), in addition to hematite, by the following reaction:

$$2Ca(Mg_{0.5},Fe_{0.5})(CO_3)_{2(solid)} + 3FeCl_{3(aq)} + 4ZnCl_4^{-2}(aq) + 2SiO_{2(aq)} + 14H^{+}_{(aq)} + 11H_2O = 2Fe_2O_{3(solid)} + 2Zn_2SiO_{4(solid)} + 25HCl_{(aq)} + 2Ca^{+2}_{(aq)} + Mg^{+2}_{(aq)} + 4CO_{2(gas)} + 5/2O_{2(gas)}. \quad (2)$$

These reactions account for the elemental losses in Ca and Mg documented using the isocon diagrams and mineralogical observations, most likely due to dissolution of the carbonates by the acidic, mineralizing fluid. By dissolving the carbonates, and mixing with meteoric water, the fluid may have increased in pH, favoring willemite precipitation. It is also possible for hematite and willemite to precipitate directly from the mixed fluids with limited interaction with the host carbonates, such as in the veinlets and breccia matrix, as shown in the following reactions:

$$2ZnCl_4^{-2}(aq) + SiO_{2(aq)} + 4H^{+}_{(aq)} + 2H_2O = Zn_2SiO_{4(solid)} + 8HCl_{(aq)} \quad (3)$$

$$2FeCl_{3(aq)} + 3H_2O = Fe_2O_{3(solid)} + 6HCl_{(aq)}. \quad (4)$$

The fact that the abundance of As, Ag, Cd, Cu, Fe, Ga, Ge, Hg, In, Mo, Ni, Pb, Sb, Se, and V increased significantly during the formation of type 3 and 4 breccias, suggests that mixing of the hydrothermal fluids favored the precipitation of these elements, and/or that the more oxidizing fluids were also important carriers for these elements. Many of the ore related elements in the Northern Extension deposit (i.e., As, Ag, Cd, Cu, Hg, Mo, Ni, Sb, Se, and V, Zn) are commonly enriched in black shales (Vine and Tourtelot, 1970; Hubert et al., 1992; Orberger et al., 2003). One of the possible sources in the Vazante region are the dark gray to black phyllites of the Serra do Garrote Formation. The mineralizing event occurred during the D_2 deformation of the Brasiliano orogeny. This may have favored the devolatilization of the basinal brines and promoted their circulation, similar to what have been documented in similar settings (Cathles and Adams, 2005). During this orogenic event, penetrative D_2 crenulation, coeval with folding formed in the pelitic units, such as the Serra do Garrote phyllites along with faulting in the dolomitic units of the Serra do Poço Verde Formation. The rheological behavior of the phyllites and dolomites during deformation may have generated interbedded permeability allowing for more pervasive circulation of hydrothermal fluids favoring leaching of these elements. The mineralized fluids were then focalized along the major NE-trending fault zones that formed during this event. Unfortunately, it was not possible to test the hypothesis of the Serra do Garrote phyllites being the source of ore-related elements during this study as outcrops were substantially weathered and few drill core intervals intercepted this unit. The low quantity of sphalerite in the breccias are explained by the low sulfur content in the hydrothermal system, oxidizing (hematite stable) and alkaline conditions of the fluids and/or lack of reductants in the site of deposition, according to the predictions from the numerical geochemical modeling by Brugger et al.(2003).

After the formation of the type 4 breccia, late hydrothermal fluids containing some reduced sulfur, base metals, and silver moved through the Type 4 breccia and precipitated some minor sulfides upon cooling. Much later, when the willemite was exposed close to the surface, supergene processes would have oxidized and dissolved the willemite and precipitated hydrozincite, smithsonite, and other zinc-oxides in the late structures.

8.2. Comparison between Vazante Group orebodies

When compared to the research conducted by Monteiro et al. (1999, 2006, 2007) on the main orebodies of the Vazante deposit, the Northern Extension ore bodies show many similarities. Both deposits are hosted in carbonates of the Lower Pamplona Member, structurally controlled, dominated by willemite mineralization, and have a strong Ag, Cd, Pb, Zn geochemical signature (Monteiro et al., 1999, 2006, 2007; Slezak, 2012).

The Northern Extension orebodies do not show the same ductile deformation recorded by Monteiro et al. (1999) in the Vazante deposit, but instead is mainly controlled by brittle deformation. Hitzman et al. (2003), and Monteiro et al. (1999, 2006, 2007) documented sphalerite in pods that were imbricated with the willemite ore, but very little sphalerite has been observed in the Northern Extension willemite ore except for small amounts located in late sulfide veinlets, indicating that the ore fluid in the Northern Extension may have evolved into a higher pH fluid, more oxidizing and/or was poorer in sulfur. In addition to the strong Ag, Cd, Pb, Zn signature, Monteiro et al. (2007) also documented gains in Rb in the mineralized breccia.

In this study, it was observed that Rb was lost during the formation of the breccias.

As mentioned previously the Vazante Group hosts other types of zinc deposits (i.e., Morro Agudo, Ambrósia and Fagundes), which are interpreted to be lead–zinc sulfide MVT/Irish-type deposits hosted in the Morro do Calcário Formation and formed during the Brasiliano orogenic event (Dardenne, 2000; Dardenne and Freitas-Silva, 1999; Monteiro et al., 2006, 2007). Although they formed during the same orogenic event and have similar geochemical signatures, the ore is composed mainly of sulfides. This difference is probably due to the distinct conditions in the deposition site, such as reduced sulfur being available in the host rocks in northern part of the Vazante basin to form the sulfide deposits, and being absent in the southern part, where the zinc silicate deposits formed (Slezak, 2012).

8.3. Comparison with other hypogene zinc silicate deposits

The Vazante Northern Extension deposit has many similarities with other hypogene zinc silicate deposits, whose characteristics are summarized in Table 1 (see references therein). As for the other currently known zinc silicate deposits, they are all hosted in carbonate rocks that formed during the Neoproterozoic to Cambrian, contain willemite and hematite as the major minerals in the ore zone, are enriched in Be, Cd, Cu, Ge, Pb and V, and some in Ag (e.g., Star Zinc and Vazante Northern Extension: Boni et al., 2011; Slezak, 2012). Many of the deposits are found in regional orogenic belts such as the Vazante and Northern Extension deposits in the Brasília Fold Belt, the Star Zinc and Kabwe in the Lufilian-Zambezi Belts, Berg Aukas and Abenab West in the Damara Orogen, and Beltana in the Flinders Range (Boni et al., 2011; Groves et al., 2003; Kamona and Friedrich, 2007; Monteiro et al., 1999; Scheider et al., 2008; Slezak, 2012). Some deposits, such as Star Zinc, contain ore textures that are very similar to those ones found in the Vazante North Extension zones (e.g. willemite as hexagonal crystal masses and fibrous splays), indicating episodic precipitation of hematite and willemite (Boni et al., 2011). Based on fluid inclusion studies in these deposits, willemite is interpreted to have precipitated from low to moderate temperature fluids (65 to 180 °C) of variable salinities (3–15 eq. wt.% NaCl). In the Vazante Northern Extension and Kabwe deposits, brecciation is interpreted to be related to major faults (Dardenne, 2000; Kamona and Friedrich, 2007; Slezak, 2012); whereas the breccias at Beltana are associated with karst (Groves et al., 2003). These similarities strongly suggest that these deposits may have formed by very similar processes, involving mixing of metalliferous saline fluids poor in sulfur (e.g., basinal brines) with more oxidizing fluids (e.g., meteoric waters).

8.4. Guidelines for exploration

Based on the characteristics of the hypogene zinc silicate deposits studied in the Vazante region and those of other deposits described in the literature, the following guidelines are proposed for their exploration. Hypogene zinc silicate deposits should be preferentially explored in Neoproterozoic to Cambrian carbonate rocks that formed in epicontinental basins along shallow passive margins, containing sequences of carbonate rocks (fluid trap) and black shales/phyllites (possible source for ore-related elements). These basins must have subsequently undergone deformation during major orogenic events forming tectonic belts (e.g., Brasília Fold Belt, Zambezi Belt, and Flinders Range). The orogenic event created and reactivated structures suitable as ore fluid conduits along which mixing can occur, causes metamorphism which can lead to the devolatilization of the salt layers forming the saline brines, and provides the energy to circulate the saline fluids upward and the topographic headings to promote downward circulation of oxidizing meteoric water.

On a district and local scale, shallow brittle fault zones and breccias associated with regional folds and faults (e.g., detachment faults caused by flexural folding) should be targeted as they create a favorable environment for mixing between basinal saline fluids and oxidizing meteoric waters. Stratigraphic contacts are important for controlling fault propagation, fluid flow, and mineral precipitation. The elements Ag, Be, Cd, Cu, Ge, Pb and V should be used as district and local scale pathfinder elements for geochemical analyses. With respect to the Vazante Northern Extension deposit, distal alteration containing enrichment in Ag, Cd, Pb, and Zn is characterized by iron-carbonates and hematite in the areas surrounding the ore breccia. Higher concentrations of Ag, As, Ba, Be, Bi, Cu, Fe, Ge, Hg, In, Mo, Ni, Pb, S, Sb, U, V, W, and Zn and the abundance of hematite in breccias indicate sites of fluid mixing and proximity to the willemite ore zones. As willemite and hematite, the most abundant phases in the ore breccia, are denser than (e.g., 3.9 to 4.2 and ~5.2 g/cm^3, respectively), the major mineral components of the host rocks (2.7 to 3.2 g/cm^3) gravimetric surveys could be used to identify orebodies at depth.

9. Conclusions

1) The Northern Extension orebodies are hosted in Neoproterozoic dolomitized carbonates, deposited in an intertidal to supratidal environment in a passive margin.
2) The Northern Extension area has undergone several phases of brittle deformation and fluid flow leading to the formation of the silicate zinc ore in tectonic-hydrothermal breccias controlled by the Vazante Northern Extension Fault Zone during the second (D_2) regional folding and associated faulting event.
3) The tectonic-hydrothermal breccias can be classified into four distinct types. Listed from the earliest to latest these are:
   a) Type 1 — Distally located from the willemite ore, weakly brecciated with some Fe-carbonate alteration.
   b) Type 2 — Strong Fe-carbonate alteration, intense brecciation.
   c) Type 3 — Hematite replacement breccia, usually proximal to the type 4 breccia.
   d) Type 4 — Willemite ore breccia, containing multiple willemite generations as well as hematite and franklinite.
4) The main mineralizing event contains hypogene willemite ore; however, late Pb–Zn and Ag–Cu sulfide veinlets were documented cross-cutting the type 4 breccia.
5) All hydrothermally altered zones at the Northern Extension deposit contain distinctly higher concentrations of Ag, Cd, Pb, and Zn than the unaltered host rocks. Moreover, the type 3 breccia has the highest average values for As, Ba, Be, Bi, Fe, Ge, In, Mo, Ni, Sb, U, V, and W, and the type 4 breccia is also enriched in these elements and yielded the highest average values for Ag, Cu, Hg, Pb, S, Se, SiO_2, and Zn. Types 3 and 4 breccias underwent losses in Ca and Mg due to replacement of carbonates in the system.
6) These mineralogical and geochemical characteristics of the ore breccias are consistent with the model of mixing between saline basinal fluids with meteoric water, similar to the model proposed by the Vazante Deposit.

Acknowledgments

We gratefully acknowledge Votorantim Metals and its staff for their support during field work, and for their insightful discussions on the geology of the Vazante area and its mineral deposits. P. Slezak thanks the Society of Economic Geologists (SEG) for his student research grant and Queen's for the graduate scholarships. This research and graduate scholarship were also supported by NSERC grants to G. Olivo. We would also like to thank L. Monteiro for sharing her knowledge on the Vazante deposits during field work, M. Appold, M. Boni, K. Kyser, H. Jamieson and P. Sry for input in the earlier versions of this manuscript, and N. Dunbar and A. Grant for assisting during EMPA and SEM analyses. We would lastly like to thank the two anonymous reviewers from Ore Geology Reviewers and the editor Franco Pirajno for providing valuable insights that helped in greatly improving this contribution.

Appendix A

Table A1
Composition of hydrothermal dolomite from type 2 and 4 breccias and veins/veinlets in the Middle Pamplona (MP) member. Analyses from electron microprobe (methodology described in Slezak, 2012).

Comment	Description	CO_2	MgO	CaO	SiO_2	MnO	FeO	ZnO	SrO	BaO	Total
20-295-01	Type 2 breccia	46.97	19.30	30.15	0.00	0.12	3.31	0.10	0.01	0.02	99.99
20-295-02	Type 2 breccia	46.79	19.17	30.24	0.00	0.16	3.25	0.15	0.11	0.12	99.98
20.295.-03	Type 2 breccia	46.52	19.32	30.59	0.00	0.14	3.21	0.06	0.04	0.12	99.99
20-295-04	Type 2 breccia	47.25	20.91	30.64	0.00	0.18	0.79	0.14	0.00	0.00	99.89
20-295-05	Type 2 breccia	43.53	22.94	33.23	0.01	0.02	0.13	0.05	0.00	0.05	99.95
20-295-06	Type 2 breccia	46.94	21.62	30.72	0.00	0.05	0.18	0.24	0.05	0.19	99.99
20-295-07	Type 2 breccia	47.80	20.91	29.99	0.00	0.16	1.02	0.05	0.00	0.05	99.97
20-295-08	Type 2 breccia	47.04	21.32	30.29	0.01	0.09	0.91	0.16	0.04	0.14	100.00
20-295-09	Type 2 breccia	47.43	20.97	30.27	0.00	0.09	1.17	0.00	0.04	0.02	99.99
20-295-010	Type 2 breccia	47.21	20.98	30.66	0.00	0.12	0.45	0.52	0.00	0.02	99.96
20-295-013	Type 2 breccia	47.56	20.58	30.54	0.00	0.05	0.88	0.34	0.04	0.00	99.99
20-295-014	Type 2 breccia	46.98	20.81	30.67	0.01	0.06	0.96	0.44	0.00	0.05	99.97
20-295-015	Type 2 breccia	46.53	20.70	31.38	0.00	0.06	0.75	0.44	0.02	0.00	99.88
20-295-016	Type 2 breccia	46.86	21.34	31.33	0.02	0.07	0.27	0.01	0.02	0.07	100.00
20-295-017	Type 2 breccia	47.05	21.42	31.14	0.01	0.05	0.11	0.08	0.00	0.12	99.96
124-75-018	Type 4 breccia	46.46	20.10	30.51	0.02	0.11	0.51	1.91	0.00	0.39	100.00
124-75-019	Type 4 breccia	45.55	16.94	33.02	0.02	0.06	1.83	2.55	0.00	0.00	99.96
124-75-020	Type 4 breccia	46.75	19.49	29.54	0.08	0.10	1.07	2.62	0.05	0.31	100.00
60-136B-033	Type 4 breccia	46.54	19.64	29.62	0.00	0.27	1.68	2.15	0.00	0.00	99.89
60-136B-034	Type 4 breccia	47.09	18.87	29.16	0.00	0.10	2.01	2.71	0.02	0.00	99.95
60-136B-035	Type 4 breccia	47.18	19.76	29.25	0.00	0.08	1.44	1.91	0.07	0.31	100.00
60-136B-036	Type 4 breccia	47.15	19.42	29.19	0.00	0.16	2.10	1.82	0.02	0.00	99.87
127-108.5-028	Type 4 breccia	46.96	18.11	28.41	0.04	0.18	2.21	4.02	0.02	0.00	99.95
127-108.5-029	Type 4 breccia	45.49	18.57	27.89	0.20	0.18	5.24	2.37	0.05	0.00	99.98
127-108.5-030	Type 4 breccia	46.78	18.37	28.34	0.01	0.09	1.86	4.44	0.05	0.00	99.93
127-108.5-031	Type 4 breccia	48.14	19.90	27.61	0.50	0.13	1.57	1.97	0.09	0.10	100.00
127-108.5-032	Type 4 breccia	46.01	18.88	28.50	0.38	0.10	2.39	3.36	0.10	0.28	100.00
141-16-09	Vein in MP	46.92	20.62	30.24	0.00	0.08	1.91	0.21	0.00	0.00	99.98
141-16-010	Vein in MP	46.37	21.14	30.55	0.53	0.08	0.93	0.11	0.01	0.29	100.00
141-16-011	Vein in MP	46.50	20.29	30.59	0.01	0.27	2.18	0.01	0.05	0.00	99.91
141-16-012	Vein in MP	45.74	20.78	30.08	2.27	0.08	0.80	0.15	0.00	0.07	99.97
141-16-013	Vein in MP	47.22	21.38	30.20	0.00	0.08	1.04	0.00	0.00	0.00	99.92
141-16-016	Vein in MP	46.62	21.04	31.01	0.04	0.07	1.01	0.02	0.00	0.00	99.80
141-16-017	Vein in MP	46.71	20.67	30.34	0.09	0.06	1.24	0.76	0.01	0.14	100.00
141-16-018	Vein in MP	47.15	20.05	30.12	0.03	0.07	1.89	0.63	0.06	0.00	100.00
141-16-020	Vein in MP	44.73	20.28	29.71	4.04	0.06	0.97	0.07	0.00	0.00	99.86
141-16-021	Vein in MP	46.44	19.88	30.10	0.02	0.06	2.15	1.25	0.05	0.00	99.95
141-16-022	Vein in MP	46.09	20.46	30.42	0.00	0.08	2.22	0.70	0.00	0.00	99.96
141-16-023	Vein in MP	46.53	20.34	30.34	0.00	0.08	1.76	0.70	0.00	0.24	99.98
141-16-024	Vein in MP	46.42	21.31	30.08	1.28	0.05	0.50	0.10	0.00	0.21	99.96
141-16-025	Vein in MP	46.67	21.29	31.16	0.13	0.08	0.47	0.09	0.00	0.02	99.92
141-16-026	Vein in MP	46.33	21.45	31.35	0.00	0.06	0.54	0.13	0.00	0.05	99.92
141-16-027	Vein in MP	46.76	20.76	30.35	0.03	0.18	1.50	0.04	0.00	0.26	99.87
141-16-028	Vein in MP	46.69	21.62	31.55	0.01	0.08	0.00	0.00	0.00	0.00	99.94
141-16-029	Vein in MP	46.43	20.39	30.28	0.00	0.19	2.32	0.00	0.02	0.36	99.99
141-16-030	Vein in MP	47.17	20.47	30.42	0.01	0.16	1.58	0.12	0.00	0.00	99.93
141-16-031	Vein in MP	47.00	20.67	31.54	0.00	0.19	0.43	0.06	0.03	0.10	100.00
141-16-032	Vein in MP	46.86	20.82	30.57	0.00	0.10	1.25	0.05	0.04	0.00	99.69
141-18-01	Veinlet in MP	46.31	20.71	30.68	0.00	0.15	1.97	0.00	0.04	0.00	99.85
141-18-02	Veinlet in MP	46.71	21.29	30.89	0.00	0.14	0.74	0.02	0.00	0.00	99.78
141-18-03	Veinlet in MP	45.93	20.04	30.77	0.00	0.06	2.91	0.00	0.00	0.00	99.71
141-18-04	Veinlet in MP	46.42	20.51	30.71	0.01	0.04	2.09	0.12	0.03	0.07	100.00
141-18-05	Veinlet in MP	46.48	20.61	30.60	0.00	0.04	2.00	0.07	0.01	0.19	99.99
141-18-06	Veinlet in MP	45.92	19.76	30.49	0.01	0.06	3.58	0.04	0.00	0.14	100.00
141-18-07	Veinlet in MP	45.53	20.16	30.93	0.01	0.01	3.10	0.01	0.02	0.24	100.00
141-18-08	Veinlet in MP	46.40	21.39	31.01	0.03	0.16	0.87	0.06	0.00	0.07	99.99
141-61-01	Veinlet in MP	46.90	21.37	30.31	0.00	0.11	1.03	0.04	0.02	0.00	99.79
141-61-02	Veinlet in MP	46.54	21.52	31.04	0.00	0.03	0.56	0.00	0.02	0.00	99.71
141-61-03	Veinlet in MP	47.57	20.87	30.20	0.00	0.10	1.04	0.11	0.01	0.00	99.91
141-61-04	Veinlet in MP	47.16	21.19	30.77	0.00	0.08	0.72	0.00	0.00	0.02	99.94
141-61-05	Veinlet in MP	47.28	21.45	30.54	0.01	0.05	0.54	0.00	0.02	0.00	99.89
141-61-06	Veinlet in MP	46.54	21.56	30.80	0.01	0.04	0.50	0.00	0.06	0.00	99.50
141-61-07	Veinlet in MP	46.58	21.67	31.01	0.00	0.05	0.48	0.03	0.00	0.12	99.93
141-61-08	Veinlet in MP	46.50	20.99	30.88	0.00	0.14	1.23	0.05	0.02	0.19	99.99
141-61-09	Veinlet in MP	46.91	21.55	30.95	0.00	0.16	0.18	0.06	0.00	0.10	99.91
141-61-014	Veinlet in MP	46.28	20.94	30.82	0.00	0.17	1.61	0.04	0.05	0.00	99.90
141-61-015	Veinlet in MP	46.54	20.94	30.54	0.00	0.18	1.72	0.03	0.04	0.00	100.00
141-61-016	Veinlet in MP	46.29	21.61	31.28	0.00	0.18	0.44	0.02	0.00	0.00	99.80
141-61-017	Veinlet in MP	41.50	23.70	34.13	0.01	0.17	0.18	0.08	0.06	0.17	100.00
141-61-018	Veinlet in MP	46.68	21.37	31.09	0.00	0.20	0.60	0.01	0.04	0.00	99.99
141-61-019	Veinlet in MP	46.28	20.82	31.06	0.04	0.21	1.50	0.04	0.00	0.00	99.95
141-61-020	Veinlet in MP	46.04	20.50	30.74	0.00	0.28	1.93	0.02	0.00	0.40	99.92

Table A2
Composition of the various generations of willemite from the type 4 breccia. Analyses from electron microprobe (methodology described in Slezak, 2012).

Comment	Description	SiO_2	ZnO	Cr_2O_3	MnO	FeO	Total
101-138-03	Gen. 1	27.51	71.04	0.05	0.00	0.18	98.78
101-138-04	Gen. 1	27.17	72.41	0.03	0.01	0.11	99.72
101-138-05	Gen. 1	27.40	72.89	0.02	0.00	0.16	100.47
101-138-06	Gen. 1	27.63	72.39	0.00	0.00	0.18	100.19
101-138-07	Gen. 1	27.27	72.41	0.01	0.00	0.14	99.83
101-138-08	Gen. 1	27.35	72.67	0.00	0.00	0.56	100.59
101-138-09	Gen. 1	27.44	72.31	0.00	0.04	0.45	100.24
101-138-10	Gen. 1	26.93	72.26	0.03	0.00	0.68	99.90
101-138-11	Gen. 1	27.18	72.75	0.03	0.00	0.49	100.44
124-75-01	Gen. 1	27.34	73.05	0.00	0.00	0.20	100.60
124-75-02	Gen. 1	27.26	72.93	0.01	0.00	0.02	100.22
124-75-03	Gen. 1	27.43	72.86	0.00	0.00	0.26	100.54
124-75-05	Gen. 1	27.28	72.21	0.00	0.00	0.11	99.60
124-75-06	Gen. 1	27.45	72.79	0.00	0.01	0.13	100.37
124-75-07	Gen. 1	27.45	73.00	0.00	0.00	0.08	100.53
124-75-08	Gen. 1	27.28	73.67	0.00	0.00	0.16	101.11
124-75-09	Gen. 1	27.39	72.76	0.00	0.00	0.07	100.23
124-75-010	Gen. 1	27.51	72.77	0.04	0.00	0.13	100.45
124-75-011	Gen. 1	27.50	72.54	0.01	0.01	0.25	100.30
124-75-012	Gen. 1	27.01	71.54	0.00	0.02	0.13	98.69
124-75-013	Gen. 1	27.25	71.83	0.02	0.00	0.15	99.24
124-75-014	Gen. 1	27.48	72.48	0.00	0.00	0.11	100.07
124-75-015	Gen. 1	27.12	71.81	0.00	0.00	0.09	99.01
124-75-016	Gen. 1	27.50	72.61	0.00	0.00	0.10	100.22
124-75-017	Gen. 1	27.62	72.71	0.00	0.00	0.07	100.39
101-138-01	Gen. 2	27.10	71.17	0.00	0.00	0.23	98.51
101-138-02	Gen. 2	27.27	71.67	0.00	0.00	0.16	99.09
60-136B-01	Gen. 2	27.37	72.48	0.00	0.00	0.35	100.20
60-136B-02	Gen. 2	27.45	72.37	0.00	0.00	0.30	100.13
60-136B-03	Gen. 2	27.26	72.18	0.00	0.00	0.39	99.83
60-136B-04	Gen. 2	27.46	72.49	0.00	0.00	0.40	100.36
60-136B-05	Gen. 2	27.30	72.01	0.00	0.00	0.37	99.68
60-136B-06	Gen. 2	27.31	72.53	0.02	0.00	0.26	100.12
60-136B-07	Gen. 2	27.40	72.60	0.00	0.00	0.18	100.19
60-136B-08	Gen. 2	27.37	73.21	0.00	0.00	0.15	100.73
60-136B-09	Gen. 3	27.46	73.16	0.00	0.05	0.13	100.80
60-136B-10	Gen. 3	27.30	72.95	0.00	0.00	0.21	100.46
60-136B-11	Gen. 3	27.29	72.64	0.00	0.00	0.19	100.11
60-136B-12	Gen. 2	27.44	73.04	0.01	0.00	0.19	100.67
60-136B-13	Gen. 2	27.43	73.19	0.00	0.00	0.22	100.84
60-136B-14	Gen. 2	27.55	72.98	0.00	0.00	0.20	100.73
60-136B-15	Gen. 2	27.60	72.73	0.01	0.00	0.21	100.55
60-136B-16	Gen. 2	27.30	72.47	0.00	0.00	0.25	100.02
60-136B-17	Gen. 2	27.17	72.42	0.00	0.00	0.59	100.18
60-136B-18	Gen. 2	27.54	72.52	0.00	0.00	0.31	100.37
60-136B-19	Gen. 2	27.51	72.58	0.00	0.00	0.27	100.35
60-136B-20	Gen. 2	27.49	72.20	0.01	0.00	0.28	99.97
60-136B-21	Gen. 2	27.44	72.03	0.03	0.00	0.16	99.66
60-136B-22	Gen. 2	27.23	71.64	0.00	0.00	0.18	99.06
60-136B-23	Gen. 2	27.20	71.75	0.02	0.00	0.21	99.18
60-136B-24	Gen. 2	27.24	71.29	0.01	0.00	0.13	98.66
60-136B-25	Gen. 2	27.15	71.23	0.04	0.00	0.19	98.61
60-136B-26	Gen. 2	27.24	71.99	0.00	0.00	0.15	99.38
60-136B-27	Gen. 2	27.36	72.66	0.00	0.00	0.29	100.31
60-136B-28	Gen. 2	27.35	72.84	0.00	0.00	0.29	100.47
60-136B-29	Gen. 2	27.13	72.39	0.03	0.00	0.97	100.51
60-136B-30	Gen. 2	27.26	72.81	0.01	0.00	0.66	100.73
60-136B-31	Gen. 2	27.30	73.17	0.00	0.00	0.08	100.55
60-136B-32	Gen. 2	27.32	73.02	0.01	0.00	0.43	100.78
60-136A-011	Gen. 2	27.17	71.83	0.02	0.00	0.73	99.76
60-136A-012	Gen. 2	27.30	71.68	0.00	0.00	0.59	99.57
60-136A-013	Gen. 2	27.21	72.58	0.02	0.00	0.50	100.31
127-108.5-01	Gen. 3	27.22	72.96	0.00	0.00	0.34	100.53
127-108.5-03	Gen. 3	27.10	72.37	0.00	0.00	0.33	99.80
127-108.5-04	Gen. 3	27.23	72.66	0.00	0.00	0.31	100.20
127-108.5-05	Gen. 3	27.50	72.71	0.00	0.00	0.18	100.39
127-108.5-06	Gen. 3	27.27	72.42	0.00	0.00	0.22	99.91
127-108.5-07	Gen. 3	27.32	72.74	0.00	0.00	0.33	100.38
127-108.5-08	Gen. 3	26.98	72.45	0.02	0.00	0.31	99.75
127-108.5-09	Gen. 3	27.35	72.54	0.00	0.00	0.30	100.18
127-108.5-010	Gen. 3	27.10	72.76	0.01	0.00	0.08	99.95
127-108.5-011	Gen. 3	27.45	72.43	0.00	0.00	0.41	100.29
127-108.5-012	Gen. 3	27.21	72.15	0.00	0.00	0.41	99.77
127-108.5-013	Gen. 3	27.45	72.56	0.00	0.00	0.40	100.41
127-108.5-014	Gen. 3	27.22	72.64	0.00	0.04	0.36	100.26
127-108.5-015	Gen. 3	27.31	72.72	0.00	0.01	0.30	100.34
127-108.5-016	Gen. 3	27.51	72.12	0.00	0.00	0.36	99.99
127-108.5-017	Gen. 3	27.42	72.92	0.01	0.00	0.59	100.94
127-108.5-018	Gen. 3	27.42	72.77	0.01	0.01	0.33	100.54
127-108.5-019	Gen. 3	27.43	72.48	0.00	0.00	0.35	100.26
127-108.5-020	Gen. 3	27.22	72.30	0.02	0.00	0.33	99.87
127-108.5-021	Gen. 3	27.16	71.92	0.00	0.00	0.66	99.73

Table A3
Composition of sphalerite from late veinlets in the type 4 breccia, the sulfide breccia in drill hole VZMIF 088, and veinlets in the Middle Pamplona (MP) member. Analyses from electron microprobe (methodology described in Slezak, 2012).

Comment	Description	S	Zn	Mn	Fe	Cd	Total
60-136A-01	Type 4 breccia	32.42	63.37	0.00	0.02	3.04	98.85
60-136A-02	Type 4 breccia	32.44	63.59	0.00	0.02	2.91	98.95
60-136A-03	Type 4 breccia	32.28	63.36	0.00	0.05	2.88	98.56
60-136A-04	Type 4 breccia	32.23	63.22	0.00	0.03	3.01	98.49
60-136A-05	Type 4 breccia	32.55	62.16	0.00	0.02	2.91	97.64
60-136A-06	Type 4 breccia	32.19	63.59	0.00	0.01	3.01	98.80
60-136A-07	Type 4 breccia	32.51	63.00	0.00	0.02	2.88	98.41
60-136A-08	Type 4 breccia	32.44	63.36	0.00	0.00	3.09	98.89
60-136A-09	Type 4 breccia	32.41	62.82	0.00	0.03	2.93	98.19
60-136A-010	Type 4 breccia	32.39	63.00	0.00	0.07	3.10	98.55
88-68-01	Sulfide breccia	32.92	66.87	0.00	0.22	0.24	100.25
88-68-02	Sulfide breccia	32.89	67.26	0.00	0.23	0.22	100.59
88-68-03	Sulfide breccia	32.86	66.98	0.00	0.24	0.24	100.32
88-68-04	Sulfide breccia	33.07	67.16	0.00	0.21	0.19	100.62
88-68-05	Sulfide breccia	32.90	67.13	0.00	0.24	0.21	100.48
88-68-06	Sulfide breccia	32.91	67.07	0.00	0.21	0.17	100.36
88-68-07	Sulfide breccia	33.04	67.08	0.00	0.25	0.24	100.61
88-68-08	Sulfide breccia	32.64	67.49	0.00	0.23	0.21	100.56
88-68-09	Sulfide breccia	32.92	67.37	0.00	0.19	0.21	100.69
88-68-010	Sulfide breccia	33.02	66.85	0.00	0.19	0.21	100.27
88-68-011	Sulfide breccia	33.01	67.24	0.00	0.29	0.16	100.69
88-68-012	Sulfide breccia	33.02	67.23	0.00	0.20	0.25	100.70
141-16-02	Vein in MP	33.48	66.29	0.00	1.10	0.39	101.26
141-16-03	Vein in MP	32.69	66.01	0.00	1.19	0.31	100.19
141-16-04	Vein in MP	32.92	66.43	0.00	1.14	0.30	100.79
141-16-05	Vein in MP	32.84	66.27	0.00	1.17	0.33	100.62
141-16-06	Vein in MP	32.83	66.56	0.00	1.17	0.34	100.90
141-16-07	Vein in MP	32.87	66.28	0.00	1.17	0.34	100.66
141-16-08	Vein in MP	32.93	66.17	0.00	1.13	0.30	100.54

Appendix B

Table B1
49 element analyses of type 1 breccia samples using 4-acid digestion, AAS for Hg, ICP-AES for As, and ICP-MS for all other elements. BH = hydrothermal breccia.

Sample		115-150	129-160	15-382	124-72	124-83	139-314	123-127	43-213	M124-284	M124-289	M124-300	M124-356
Geologic unit		BH	BH	BH	BH	BH	BH	BH	BH	BH	BH	BH	BH
Description		Type 1	Type 1	Type 1	Type 1	Type 1	Type 1	Type 1	Type 1	Type 1	Type 1	Type 1	Type 1
Ag	ppm	3	2.31	0.13	0.46	0.25	0.07	0.1	0.06	0.1	0.18	0.18	0.15
Al	%	0.34	1.21	0.62	0.92	0.3	0.53	0.41	0.49	0.41	0.41	0.33	0.18
As	ppm	5	8	5	13	5	8	5	5	5	7	5	5
Ba	ppm	50	200	120	30	10	20	40	350	30	70	20	20
Be	ppm	0.05	0.55	0.2	0.26	0.15	0.3	0.3	0.3	0.15	0.26	0.09	0.09
Bi	ppm	0.08	0.07	0.03	0.02	0.02	0.03	0.03	0.02	0.02	0.04	0.01	0.01
Ca	%	19.05	16.35	19.05	18.05	20.3	19.25	19.7	19.45	19.1	17.25	19.3	20.1
Cd	ppm	278	11.05	5.53	553	145.5	289	4.84	36.8	158.5	4.94	22.2	236
Ce	ppm	2.64	17.1	6.29	14.7	3.29	5.73	5.25	6.4	3.48	6.29	3.42	3.16
Co	ppm	31.3	18.4	3.5	57.4	19.6	65.6	1.5	17.5	15.6	6	6.6	28.6
Cr	ppm	6	8	4	8	3	3	6	2	4	4	3	2
Cs	ppm	0.1	0.74	0.5	0.16	0.12	0.31	0.43	0.51	0.16	0.32	0.17	0.09
Cu	ppm	18	15.7	4.6	15.9	5.6	2.5	3.8	1.8	6.2	9.1	6.7	3.1
Fe	%	1.31	1.34	0.69	2.26	1.04	1.2	0.35	0.71	0.95	2.76	0.57	0.84
Ga	ppm	1.3	3.39	1.71	3.46	1.2	1.84	1.01	1.35	1.29	1.1	0.68	0.66
Ge	ppm	0.05	0.05	0.07	0.12	0.1	0.12	0.12	0.12	0.12	0.13	0.11	0.11
Hf	ppm	0.2	0.5	0.3	0.4	0.1	0.4	0.3	0.2	0.1	0.1	0.2	0.1
Hg	ppm	0.31	0.07	0.01	0.02	0.07	0.16	0.04	0.03	0.04	0.1	0.14	0.02
In	ppm	0.01	0.033	0.006	0.064	0.012	0.139	0.006	0.006	0.005	0.006	0.005	0.047
K	%	0.02	0.54	0.35	0.01	0.01	0.02	0.21	0.23	0.08	0.2	0.04	0.02
La	ppm	1.7	8	3.1	9.2	2	3.6	2.4	3.2	1.9	2.9	1.9	2.7
Li	ppm	3.3	22.7	8.4	17.1	7.2	16.9	9.5	9.5	7.6	5.8	6.6	5.2
Mg	%	11.8	10.55	11.9	11.45	12.35	11.9	11.65	11.6	12	10.7	12.15	12.45
Mn	ppm	529	564	519	637	409	627	144	613	541	693	578	495
Mo	ppm	0.11	0.18	0.05	0.3	0.14	0.16	0.08	0.05	0.11	0.32	0.11	0.07
Na	%	0.01	0.03	0.02	0.01	0.02	0.02	0.02	0.02	0.02	0.01	0.02	0.02
Nb	ppm	0.8	2.1	1.2	1.4	0.6	1.2	1	0.9	0.5	0.5	0.4	0.3
Ni	ppm	9.1	7.1	4.7	32.3	12.3	41	2.5	7.5	9.4	5.9	3.6	10.9
P	ppm	110	1330	170	380	80	110	110	120	110	230	270	380
Pb	ppm	4730	1225	72.5	2060	1480	1410	314	656	1400	1445	740	2080
Rb	ppm	0.7	21.5	11.6	0.6	0.6	1.1	7.9	8.7	2.5	6.2	1.3	0.5
Re	ppm	0.002	0.002	0.002	0.003	0.003	0.004	0.003	0.003	0.002	0.002	0.002	0.002
S	%	0.03	0.01	0.01	0.01	0.01	0.01	0.01	0.01	0.01	0.01	0.01	0.01
Sb	ppm	0.25	1.13	0.12	1.36	0.42	0.33	0.09	0.23	0.1	0.78	0.05	0.08
Sc	ppm	0.7	2.1	1	1.8	0.6	1.2	0.8	0.8	0.7	0.6	0.5	0.4
Se	ppm	4	1	1	1	1	1	1	1	1	1	1	1
Sn	ppm	0.2	0.4	0.2	0.3	0.2	0.3	0.2	0.2	0.2	0.2	0.2	0.2
Sr	ppm	63.7	49.7	56	45.1	58.8	81.5	83.8	75.9	57.6	46.1	47.3	56
Ta	ppm	0.05	0.13	0.06	0.1	0.05	0.07	0.06	0.05	0.05	0.05	0.05	0.05
Te	ppm	0.05	0.05	0.05	0.05	0.05	0.05	0.05	0.05	0.05	0.05	0.05	0.05
Th	ppm	0.3	1.7	0.7	1.4	0.5	1	0.7	0.7	0.3	0.6	0.4	0.3
Ti	%	0.018	0.056	0.027	0.046	0.015	0.033	0.023	0.021	0.016	0.015	0.016	0.009
Tl	ppm	0.02	0.15	0.04	0.02	0.02	0.02	0.05	0.03	0.02	0.03	0.02	0.02
U	ppm	0.6	1.3	0.4	1.3	0.7	1.6	4.1	0.4	0.4	1	0.5	0.8
V	ppm	33	18	8	23	6	9	27	6	12	28	5	8
W	ppm	0.1	0.3	0.1	0.1	0.1	0.1	0.1	0.1	0.1	0.3	0.1	0.1
Y	ppm	2.1	9.4	1.9	3.9	2.1	3.7	2.4	2	1.6	3.4	1.2	1.9
Zn	ppm	19,000	3160	1470	25,700	12,250	9280	542	3660	5350	1120	6170	6740
Zr	ppm	6.3	19.9	9.3	12.7	5.3	12.7	10.1	8.4	3.7	4.7	5.4	3.4

Table B2
49 element analyses of type 2 and 3 breccia samples using 4-acid digestion, AAS for Hg, ICP-AES for As, and ICP-MS for all other elements. BH = hydrothermal breccia.

Sample		12-377	136-112	28-47	101-148	43-232	M124-347	125-55	124-62	101-128	M124-305	M124-353
Geologic unit		BH	BH	BH	BH	BH	BH	BH	BH	BH	BH	BH
Description		Type 2	Type 2	Type 2	Type 2	Type 2	Type 2	Type 3	Type 3	Type 3	Type 3	Type 3
Ag	ppm	0.84	2.91	0.1	0.41	0.03	0.31	0.99	1.01	5.59	8.82	4.92
Al	%	0.19	0.13	0.67	0.18	0.09	0.22	0.78	0.61	0.43	0.35	0.17
As	ppm	5	4.4	5	10	6	8	104	115.5	87.9	147	54.7
Ba	ppm	1980	1480	170	320	390	60	100	50	4570	50	30
Be	ppm	0.11	0.16	0.36	0.32	0.08	0.1	1.63	2.09	0.73	0.87	0.82
Bi	ppm	0.02	0.01	0.06	0.02	0.01	0.02	0.15	0.08	0.08	0.08	0.04
Ca	%	17.65	7.44	19.7	16.6	19.65	17.65	6.72	7.04	6.06	1.55	2.09
Cd	ppm	7.75	214	8.69	1110	167.5	628	108	189	335	50.7	66.5
Ce	ppm	3.59	2.54	7.59	4.71	5.76	7.41	9.78	4.96	6.32	3.78	1.56
Co	ppm	9	53.2	5.8	36.5	27.2	44	61.9	60.3	14.5	8.2	25.4
Cr	ppm	4	19	6	1	1	2	5	5	1	17	13
Cs	ppm	0.19	0.07	0.58	0.07	0.08	0.25	1	0.75	0.41	0.75	0.3
Cu	ppm	6.9	7.2	3.3	7.3	2.6	2.7	9	16.2	10.4	48.9	21.9
Fe	%	2.03	3.37	0.46	1.37	1.49	4.81	43.1	41.2	25.1	54.31	59.87
Ga	ppm	0.68	1.54	1.79	2.31	0.34	1.09	3.17	3.61	2.8	3.25	5.11
Ge	ppm	0.05	0.05	0.08	0.08	0.1	0.14	0.95	0.21	0.12	0.18	0.19
Hf	ppm	0.1	0.1	0.3	0.1	0.1	0.1	0.1	0.1	0.1	0.1	0.1
Hg	ppm	0.22	0.1	0.07	0.07	0.02	0.03	0.2	0.05	0.32	0.34	0.05
In	ppm	0.01	0.079	0.011	0.017	0.006	0.074	2.94	2.89	0.077	0.017	0.613
K	%	0.08	0.01	0.39	0.01	0.01	0.04	0.04	0.1	0.01	0.03	0.01
La	ppm	1.9	2	3.7	2.6	3.3	3.9	3.7	2.8	3.2	1.9	0.7
Li	ppm	4.3	2.8	10.8	4	3.5	5.7	10.1	13.2	3.8	3.3	3.8
Mg	%	10.95	4.06	11.8	10.1	11.65	10.9	3.97	4.28	3.54	0.88	1.33
Mn	ppm	720	1040	207	825	1080	899	451	385	671	357	165
Mo	ppm	0.22	0.48	0.13	0.14	0.1	0.49	3.87	5.25	3.81	9.29	12.7
Na	%	0.05	0.03	0.03	0.01	0.02	0.01	0.01	0.01	0.07	0.01	0.01
Nb	ppm	0.6	0.3	1.4	0.3	0.2	0.4	1.4	0.2	0.2	0.3	0.1
Ni	ppm	2.9	13.9	5.4	6.4	11.8	14.4	48.5	31.5	10.1	11.4	30
P	ppm	80	250	2700	80	160	330	260	210	320	150	60
Pb	ppm	130.5	917	187	2010	1410	2230	1850	2390	2850	2680	1160
Rb	ppm	3.4	0.2	16.7	0.5	0.4	1.4	2.7	3.6	0.7	1.5	0.3
Re	ppm	0.002	0.002	0.002	0.003	0.003	0.002	0.002	0.004	0.003	0.002	0.002
S	%	0.06	0.04	0.01	0.01	0.01	0.01	0.12	0.01	0.2	0.01	0.01
Sb	ppm	0.32	0.99	0.18	1.42	0.36	1.15	47.6	31	13.5	9.11	32.7
Sc	ppm	0.3	0.3	1	0.3	0.1	0.4	0.5	0.6	0.7	1.3	0.1
Se	ppm	1	1	1	1	1	1	3	1	1	1	1
Sn	ppm	0.2	0.2	0.3	0.2	0.2	0.2	0.2	0.3	0.2	0.2	1.1
Sr	ppm	56.3	37	70.8	28.1	75.3	75.4	16.8	20.3	444	10.4	11.3
Ta	ppm	0.05	0.05	0.09	0.05	0.05	0.05	0.05	0.05	0.05	0.05	0.05
Te	ppm	0.05	0.05	0.05	0.05	0.05	0.05	0.05	0.05	0.05	0.05	0.05
Th	ppm	0.2	0.2	1.3	0.3	0.2	0.3	0.2	0.2	0.2	0.2	0.2
Ti	%	0.009	0.006	0.026	0.008	0.005	0.011	0.005	0.005	0.006	0.007	0.005
Tl	ppm	0.02	0.02	0.07	0.02	0.02	0.02	0.02	0.04	0.02	0.02	0.02
U	ppm	0.6	0.4	0.7	0.7	0.2	1.5	7.2	15.3	4.2	4.7	6.8
V	ppm	18	97	6	17	13	10	153	146	52	49	60
W	ppm	0.3	0.3	0.1	0.1	0.1	0.2	1.2	1.1	0.8	0.4	0.5
Y	ppm	1.5	2	3.1	2.2	3.1	3.6	3.4	2	1.9	1.1	0.7
Zn	ppm	4030	5440	1180	107,000	8940	7050	24,800	12,200	45,600	46,600	5390
Zr	ppm	4.2	2.9	11.3	3.3	1.5	3.6	4.2	4.2	2.6	2.1	0.5

Table B3
49 element analyses of type 4 breccia samples using 4-acid digestion, AAS for Hg, ICP-AES for As, and ICP-MS for all other elements. BH = hydrothermal breccia.

Sample		12-347	122-75	115-220	129-167	60-120	60-136	101-137	123-73	124-75	124-78	M124-329
Geologic unit		BH	BH	BH	BH	BH	BH	BH	BH	BH	BH	BH
Description		Type 4	Type 4	Type 4	Type 4	Type 4	Type 4	Type 4	Type 4	Type 4	Type 4	Type 4
Ag	ppm	231	43.1	394	24.1	19.55	257	3.58	30	5.7	37	26.1
Al	%	0.08	0.04	0.02	0.65	0.1	0.06	0.03	0.07	0.03	0.07	0.12
As	ppm	42.4	42.5	96.6	68.5	54.7	49.3	68.1	90.2	57.3	63.9	82
Ba	ppm	1510	820	640	150	1940	1960	470	150	70	280	20
Be	ppm	0.76	0.98	0.48	1.65	0.53	0.71	0.47	0.74	0.73	1.42	2.38
Bi	ppm	0.03	0.02	0.06	0.09	0.02	0.07	0.02	0.02	0.02	0.01	0.01
Ca	%	3.04	1.19	0.17	2.15	0.6	4.53	7.01	1.56	1.84	1.27	0.43
Cd	ppm	178	59.1	89.2	222	14.55	900	812	55.3	32.5	68.5	10.55
Ce	ppm	1.56	4.21	0.74	11.8	1.44	4.55	2.17	6.23	3.6	1.54	2.27
Co	ppm	7.8	38.3	1.7	18.5	6.4	12.1	16.8	9.5	12.8	9.7	14.5
Cr	ppm	11	9	7	30	3	8	11	12	5	12	10
Cs	ppm	0.08	0.05	0.05	0.15	0.14	0.05	0.05	0.05	0.05	0.05	0.13
Cu	ppm	338	74.9	2650	132.5	77.6	191.5	16.6	62.5	18	62.5	22.1
Fe	%	3.91	3.8	1.85	12.4	13.3	7.21	1.91	15.85	6.02	12.1	13.4
Ga	ppm	5.46	1.09	1.38	6.25	1.77	3.69	4.08	1.72	1.63	3.21	2.13
Ge	ppm	0.06	0.06	0.07	0.25	0.21	0.17	0.05	0.34	0.12	0.12	0.21
Hf	ppm	0.1	0.1	0.1	0.4	0.1	0.1	0.1	0.1	0.1	0.1	0.1
Hg	ppm	8.3	1.05	8.2	0.71	2.12	0.8	0.23	1.08	0.14	1.27	0.01
In	ppm	0.082	0.828	0.061	0.285	0.677	0.086	0.008	0.231	0.532	1.935	2.1
K	%	0.03	0.01	0.01	0.01	0.01	0.01	0.01	0.01	0.01	0.01	0.01
La	ppm	0.8	2.5	0.5	5.2	0.9	2.6	1.7	3	1.7	0.9	1
Li	ppm	4.4	5.2	10.9	16.7	4	8.3	4.6	12.6	14.5	8.9	5
Mg	%	1.67	2.59	0.11	1.5	0.36	2.5	3.83	0.88	0.89	0.63	0.25
Mn	ppm	185	403	22	158	73	438	491	115	94	71	80
Mo	ppm	0.6	0.78	0.73	1.99	1.91	1.12	0.37	1.8	1.14	2.22	2.43
Na	%	0.03	0.01	0.01	0.01	0.03	0.04	0.01	0.01	0.01	0.01	0.01
Nb	ppm	0.3	0.2	0.1	1.4	0.4	0.3	0.2	0.5	0.1	0.1	0.1
Ni	ppm	3	7.1	1.2	21.3	8.3	6.6	4.3	6.1	9.3	12.8	10.1
P	ppm	110	140	240	2150	120	150	290	280	1030	1r90	400
Pb	ppm	1295	1750	87,000	2960	1295	34,700	2920	2030	1180	1290	1310
Rb	ppm	0.9	0.2	0.2	0.3	0.3	0.2	0.2	0.3	0.1	0.2	0.4
Re	ppm	0.002	0.002	0.002	0.002	0.002	0.002	0.002	0.002	0.003	0.003	0.002
S	%	0.05	0.04	0.72	0.02	0.2	0.24	0.02	0.07	0.01	0.01	0.01
Sb	ppm	2.2	5.63	1.02	12.75	2.99	2.95	1.36	12.95	3.26	11.05	4.71
Sc	ppm	0.2	0.5	0.1	1.2	0.2	0.2	0.4	0.2	0.1	0.1	0.1
Se	ppm	41	38	39	37	15	41	35	29	6	8	4
Sn	ppm	0.2	0.2	0.2	0.4	0.2	0.2	0.2	0.2	0.2	0.2	0.2
Sr	ppm	22.3	34.2	85.8	12.1	1895	86.8	17.6	39	23.7	12.5	5.7
Ta	ppm	0.05	0.05	0.05	0.07	0.05	0.05	0.05	0.05	0.05	0.05	0.05
Te	ppm	0.05	0.05	0.05	0.07	0.05	0.05	0.05	0.05	0.05	0.05	0.05
Th	ppm	0.2	0.2	0.2	0.9	0.2	0.2	0.2	0.2	0.2	0.2	0.2
Ti	%	0.005	0.005	0.005	0.03	0.005	0.005	0.005	0.005	0.005	0.005	0.005
Tl	ppm	0.02	0.02	0.02	0.02	0.02	0.02	0.02	0.02	0.02	0.02	0.02
U	ppm	1.5	0.7	0.7	7.3	3.8	3.5	0.5	3.8	1.9	8.4	2.9
V	ppm	21	8	27	47	33	76	20	138	33	94	34
W	ppm	0.2	0.2	0.2	0.5	0.2	0.3	0.1	0.4	0.1	0.4	0.2
Y	ppm	0.5	1	0.3	2.3	0.6	1.2	1.1	0.7	1.6	0.8	0.8
Zn	ppm	460,000	378,700	489,000	401,200	170,500	373,800	382,900	324,000	486,400	350,000	454,200
Zr	ppm	1.3	0.6	0.7	12.9	1	0.8	0.5	1.1	0.5	0.7	0.6

Table B4
49 element analyses of the Lower Pamplona dolostone samples using 4-acid digestion, AAS for Hg, ICP-AES for As, and ICP-MS for all other elements. LP = Lower Pamplona Member, carb = carbonate.

Sample		143-124	155-185	139-194	123-46	123-51	101-222	M124-250	139-135
Geologic unit		LP	LP	LP	LP	LP	LP	LP	LP
Description		Dolomite	Dolomite	Fe-carb alteration	Fe-carb alteration	Alteration veinlets	Alteration veinlets	Chalcedonic silica alt	Fe-carb selvage alteration
Ag	ppm	0.02	0.06	0.07	0.13	0.15	0.07	0.08	0.7
Al	%	0.93	2.48	0.51	2.22	1.43	0.4	0.58	0.7
As	ppm	5	5	5	9	17	5	5	8
Ba	ppm	90	430	130	50	40	750	160	110
Be	ppm	0.2	0.34	0.23	0.77	0.75	0.22	0.21	0.22
Bi	ppm	0.02	0.04	0.02	0.05	0.08	0.02	0.02	0.02
Ca	%	18.7	13.45	19.4	15.45	16.8	19.45	15.4	15.3
Cd	ppm	0.16	0.29	4.59	16.45	104	3.82	2.65	3.63
Ce	ppm	9.81	15	5.48	21.4	13.8	5.99	5.18	4.86
Co	ppm	2.1	2.4	2.7	14.3	42.6	16.5	0.9	2.7
Cr	ppm	9	9	3	10	7	2	11	23
Cs	ppm	0.61	1.93	0.62	1.07	0.8	0.25	0.4	0.22
Cu	ppm	2.4	3.3	2.3	5.4	10.6	9.7	4.5	17.6
Fe	%	0.73	0.66	0.74	1.14	5.11	0.95	0.5	0.99
Ga	ppm	2.32	5.08	1.3	4.75	3.72	1.25	1.4	1.59
Ge	ppm	0.05	0.14	0.1	0.13	0.11	0.06	0.11	0.13
Hf	ppm	0.4	0.7	0.3	1.2	0.7	0.2	0.3	0.2
Hg	ppm	0.1	0.1	0.04	0.69	0.07	0.06	0.04	0.13
In	ppm	0.008	0.011	0.007	0.018	0.054	0.015	0.005	0.012
K	%	0.78	2.7	0.25	0.86	0.55	0.29	0.41	0.72
La	ppm	5	7.1	2.7	10.1	7	3	2.6	2.1
Li	ppm	6.3	9.1	10	20.9	16.4	5.2	5.1	3.6
Mg	%	11.35	8.39	11.65	9.83	10.55	12.05	9.39	9.61
Mn	ppm	312	262	397	530	696	464	228	249
Mo	ppm	0.05	0.1	0.11	0.07	0.6	0.21	0.55	2.18
Na	%	0.03	0.03	0.02	0.06	0.02	0.01	0.01	0.02
Nb	ppm	1.3	2.7	0.8	2.9	2.1	1.1	0.8	0.7
Ni	ppm	4.8	4.8	3.3	9.4	24	6.6	1.4	4.5
P	ppm	90	190	100	280	90	140	60	80
Pb	ppm	3.2	9.4	195	763	2870	59.1	80.6	118.5
Rb	ppm	17.2	46.2	8.4	27.7	18.5	7.4	8	9.6
Re	ppm	0.002	0.002	0.003	0.003	0.004	0.002	0.002	0.004
S	%	0.01	0.01	0.01	0.01	0.01	0.02	0.02	0.01
Sb	ppm	0.16	0.2	0.38	0.62	3.17	0.19	0.1	0.32
Sc	ppm	1.5	2.4	0.8	3.9	2.8	0.8	0.7	0.6
Se	ppm	1	1	1	1	1	1	1	1
Sn	ppm	0.2	0.4	0.2	0.6	0.4	0.2	0.2	0.3
Sr	ppm	55.8	69.8	75.6	44.9	28.1	72.3	55	46.9
Ta	ppm	0.09	0.17	0.05	0.2	0.13	0.06	0.06	0.05
Te	ppm	0.05	0.05	0.05	0.05	0.05	0.05	0.05	0.05
Th	ppm	1.1	1.6	0.7	2.9	1.9	0.5	0.6	0.6
Ti	%	0.043	0.062	0.023	0.112	0.067	0.019	0.022	0.017
Tl	ppm	0.06	0.16	0.04	0.19	0.11	0.03	0.03	0.05
U	ppm	0.9	0.5	0.5	0.6	1.6	0.4	0.7	1
V	ppm	13	8	7	14	32	11	28	27
W	ppm	0.2	0.2	0.1	0.2	0.4	0.1	0.1	0.2
Y	ppm	3.8	6.5	2	7.7	4.7	1.8	1.9	2.3
Zn	ppm	36	24	1170	4070	9650	581	390	2140
Zr	ppm	14.8	22.8	10.3	40.7	21.3	10.7	8.6	7.4

References

Almeida, F.F.M., 1969. Evolucao tectônica do Centro-Oeste Brasileiro. An. Acad. Bras. Cienc. 280–296.

Almeida, F.F.M., Hasui, Y., Brito Neves, B.B., Fuck, R.A., 1981. Brazilian structural provinces. an introduction. Earth Sci. Rev. 17, 1–29.

Appold, M.S., Monteiro, L.V.S., 2009. Numerical modeling of hydrothermal zinc silicate and sulfide mineralization in the Vazante deposit, Brazil. Geofluids 9, 96–115.

Azmy, K., Kendall, B., Creaser, R.A., Heaman, L., Oliveira, T.F., 2008. Global correlation of the Vazante Group, São Francisco Basin, Brazil: Re–Os and U–Pb radiometric age constraints. Precambrian Res. 164, 160–172.

Bhatia, M.R., Crook, A.W., 1986. Trace element characteristics of graywackes and tectonic setting discrimination of sedimentary basins. Contrib. Mineral. Petrol. 92, 181–193.

Boni, M., Large, D., 2003. Non-sulfide Zinc mineralization in Europe: an overview. Econ. Geol. 98, 715–729.

Boni, M., Terracciano, R., Balassone, G., Gleeson, S.A., Matthews, A., 2011. The carbonate-hosted willemite prospects of the Zambezi Metamorphic Belt, Zambia. Miner. Deposita 46, 707–729.

Brugger, J., McPhail, D.C., Wallace, M., Waters, J., 2003. Formation of willemite in hydrothermal environments. Econ. Geol. 98, 819–835.

Cathles, L.M., Adams, J.J., 2005. Fluid flow and petroleum and mineral resources in the upper (<20-km) continental crust. Economic Geology 100th Anniversary Volume, pp. 77–110.

Cloud, P.E., Dardenne, M.A., 1973. Proterozoic age of the Bambuí Group in Brazil. Geol. Soc. Am. Bull. 84, 1673–1676.

Cooley, M.A., Price, R.A., Dixon, J.M., Kyser, T.K., 2011a. Along-strike variations and internal details of chevron-style, flexural slip thrust-propogation folds within the southern Livingstone Range anticlinorium, a paleohydrocarbone reservoir in southern Alberta Foothils, Canada. Am. Assoc. Pet. Geol. Bull. 95, 1821–1849.

Cooley, M.A., Price, R.A., Kyser, T.K., Dixon, J.M., 2011b. Stable-isotope geochemistry of syntectonic veins in Paleozoic carbonate rocks in the Livingstone Range anticlinorium and their significance to the thermal and fluid evolution of the southern Canadian foreland thrust and fold belt. Am. Assoc. Pet. Geol. Bull. 95, 1851–1882.

Cunha, I.A., Misi, A., Babinski, M., Iyer, S.S.S., 2007. Lead isotope constraints on the genesis of Pb–Zn deposits in the Neoproterozoic Vazante Group, Minas Gerais, Brazil. Gondwana Res. 11, 382–395.

Dardenne, M.A., 1978. Geologia da Região de Morro Agudo, Minas Gerais. Bol. Núcleo Centro-Oeste. Soc. Bras. Geol. 7–8, 68–84.

Dardenne, M.A., 2000. The Brasília Fold Belt. In: Cordan, U.G., Milani, E.J., Thomaz Filho, A., Campos, D.A. (Eds.), The Tectonic Evolution of South America. 31st International Geological Congress, Rio de Janeiro, pp. 231–263.

Dardenne, M.A., Freitas-Silva, F.H., 1999. Pb–Zn ore deposits of Bambuí and Vazante groups, in the São Francisco Craton and Brasília Fold Belt, Brazil. In: Gloria da Silva, M., Misi, A. (Eds.), Base Metal Deposits of Brazil. Salvador, Ernesto von Sperling, Salvador, pp. 75–83.

Freitas-Silva, F.H., Dardenne, M.A., 1994. Proposta de subdiviSão estratigrafica formal para o Grupo Canastra no oeste de Minas Gerais e leste de Goias. Sociedade Brasilera de Geologia, Goiana, pp. 161–163.
Grant, J.A., 1986. The isocon diagram: a simple solution to Gresen's Equation for metosomatic alteration. Econ. Geol. 81, 1976–1982.
Grant, J.A., 2005. Isocon analysis: a brief review of the method and applications. Phys. Chem. Earth. 30, 997–1004.
Groves, I.M., Carman, C.E., Dunlap, W.J., 2003. Geology of the Beltana Willemite Deposit, Flinders Range, South Australia. Econ. Geol. 98, 797–818.
Hitzman, M.W., Thorman, C.H., Romagna, G., Olivera, T.F., Dardenne, M.A., Drew, L.J., 1995. The Morro Agudo Zn–Pb deposit, Minas Gerais, Brazil: a Proterozoic Irish-type carbonate-hosted sedex-replacement deposit. Geol. Soc. Am. Abstr. Programs 27, A408.
Hitzman, M.W., Reynolds, N.A., Sangster, D.F., Allen, C.R., Carman, C.E., 2003. Classification, genesis, and exploration guides for non-sulfide zinc deposits. Econ. Geol. 98, 685–714.
Hubert, L.J., Gregoire, D.C., Paktunc, D., 1992. Sedimentary nickel, zinc, and platinum group element mineralization in Devonian black shales at the Nick property, Yukon, Canada: a new deposit type. Explor. Min. Geol. J. 1, 39–62.
Kamona, A.F., Friedrich, G.H., 2007. Geology, mineralogy, and stable isotopes of the Kabwe carbonate-hosted Pb–Zn deposit, Central Zambia. Ore Geol. Rev. 30, 217–243.
Martins-Neto, M.A., 2009. Sequence stratigraphic framework of Proterozoic successions in eastern Brazil. Mar. Pet. Geol. 26, 163–176.
Misi, A., Iyer, S.S.S., Coelho, C.E.S., Tassinari, C.C.G., Franca-Rocha, W.J.S., Cunha, I.A., Gomes, A.S.R., Oliveira, T.F., Teixeira, J.B.G., Filho, V.M.C., 2005. Sediment hosted lead–zinc deposits of the Neoproterozoic Bambuí Group and correlative sequences, São Francisco Craton, Brazil: a review and a possible metallogenic evolution model. Ore Geol. Rev. 26, 263–304.
Monteiro, L.V.S., 2002. Modelamento Metalogenético dos depósitos de Zn de Vazante, Fagundes e Ambrósia, associados ao Grupo Vazante, Minas Gerais. Unpublished Ph.D. thesis Universidade de São Paulo, São Paulo.
Monteiro, J.V.S., Bettencourt, J.S., Spiro, B., Graca, R., Oliveira, T.F., 1999. The Vazante zinc mine, Minas Gerais, Brazil: constraints on willemitic mineralization and fluid evolution. Explor. Min. Geol. J. 8, 21–42.
Monteiro, L.V.S., Bettencourt, J.S., Juliani, C., Oliveira, T.F., 2006. Geology, petrography, and mineral chemistry of the Vazante non-sulfide and Ambrosia and Fagundes sulfide-rich carbonate-hosted Zn–(Pb) deposits, Minas Gerais, Brazil. Ore Geol. Rev. 28, 201–234.
Monteiro, L.V.S., Bettencourt, J.S., Juliani, C., Oliveira, T.F., 2007. Non-sulfide and sulfide-rich zinc mineralizations in the Vazante, Ambrosia and Fagundes deposits, Minas Gerais, Brazil: Mass balance and stable isotope characteristics of the hydrothermal alterations. Gondwana Res. 11, 362–381.
Orberger, B., Pasava, J., Gallien, J.P., Daudin, L., Trocellier, P., 2003. Se, As, Mo, Ag, Cd, In, Sb, Pt, Au, Tl, Re traces in biogenic and abiogenic sulfides from black shales (Selwyn Basin, Yukon territories, Canada): a nuclear microprobe study. Nucl. Inst. Methods Phys. Res. 210, 441–448.
Pimentel, M.M., Dardenne, M.A., Fuck, R.A., Viana, M.G., Junges, S.L., Fischel, D.P., Seer, H.J., Dantas, E.L., 2001. Nd isotopes of the provenance of detrital sediments of the Neoproterozoic Brasília Belt, central Brazil. J. S. Am. Earth Sci. 14, 571–585.
Pinho, J.M.M., 1990. Evolução tectônica da mineralizacao de zinco de Vazante, Brasília. Unpublished M.Sc. thesis Universidade de Brasília, Brasília.
Pirajno, F., Joubert, B.D., 1993. An overview of carbonate-hosted mineral deposits in the Otavi Mountain Land, Namibia: implications for ore genesis. J. Afr. Earth Sci. 16, 265–272.
Préat, A., Kolo, K., Prian, J.P., Delpomdor, F., 2010. A peritidal evaporite environment in the Neoproterozoic of South Gabon (Schisto-Calcair Subgroup, Nyanga Basin). Precambrian Res. 177, 253–265.
Rigobello, A.E., Branquinho, J.A., Silva Dantas, M.G., Oliveira, T.F., Neves Filho, W., 1988. Mina de zinco de Vazante, Minas Gerais. In: Schobbenhaus, C., Coelho, C.E.S. (Eds.), Principais Depositos Minerais do Brasil: Brasília, DNPM/Companhia Vale do Rio Doce, pp. 101–110.
Riveros, P.A., Dutrizac, J.E., 1997. The precipitation of hematite from ferric chloride media. Hydrometallurgy 46, 85–104.
Rodrigues, J.B., Pimentel, M.M., Dardenne, M.A., Armstrong, R.A., 2010. Age, provenance and tectonic setting of the Canastra and Ibiá Groups (Brasília Belt, Brazil): implications for the age of a Neoproterozoic glacial event in central Brazil. J. S. Am. Earth Sci. 29, 512–521.
Rostirolla, S.P., Mancini, F., Reis Neto, J.M., Figueira, E.G., Araujo, E.C., 2002. Analise estrutural da mina de Vazante e adjacencias: Geometria, cinematica, e implicacoes para a hidrogeologia. Rev. Bras. Geosci. 32, 59–68.
Scheider, J., Boni, M., Laukamp, C., Bechstädt, T., Petzel, V., 2008. Willemite (Zn_2SiO_4) as a possible Rb–Sr geochronometer for dating nonsulfide Zn–Pb mineralization: examples from the Otavi Mountainland (Namibia). Ore Geol. Rev. 33, 152–167.
Shinn, E.A., 1968. Practical significance of birdseye structures in carbonate rocks. J. Sed. Petrogr. 38, 215–223.
Slezak, P., 2012. Geology, Mineralogy, and Geochemistry of the Vazante-Northern Extension Zinc Silicate Deposit, Minas Gerais, Brazil. Unpublished M.Sc. thesis Queen's University, Kingston.
Thomaz Filho, A., Kawashita, K., Cordani, U.G., 1998. A origem do Grupo Bambuí no contexto da evolução geotectônica e de idades radiométricas. Anais da Academia Brasileira de Ciências 70, 537–548.
Valeriano, C.M., Pimentel, M.M., Heilbron, M., Almeida, J.C.H., Trouw, R.A.J., 2008. Tectonic evolution of the Brasília Belt, Central Brazil, and early assembly of Gondwana. Geol. Soc. Lond. Spec. Publ. 294, 197–210.
Vine, J.D., Tourtelot, E.B., 1970. Geochemistry of black shale deposits — a summary report. Econ. Geol. 65, 253–272.
Warren, J.K., 2006. Evaporites: Sediments, Resources, and Hydrocarbons. Springer, Stürtz.